

A Study of Event Shapes and Determinations of α_s using data of e^+e^- Annihilations at $\sqrt{s} = 22$ to 44 GeV

P.A. Movilla Fernández⁽¹⁾, O. Biebel⁽¹⁾, S. Bethke⁽¹⁾, S. Kluth⁽²⁾, P. Pfeifenschneider⁽¹⁾
and the JADE Collaboration⁽³⁾

Abstract

Data recorded by the JADE experiment at the PETRA e^+e^- collider were used to measure the event shape observables thrust, heavy jet mass, wide and total jet broadening and the differential 2-jet rate in the Durham scheme. For the latter three observables, no experimental results have previously been presented at these energies. The distributions were compared with resummed QCD calculations ($\mathcal{O}(\alpha_s^2)$ +NLLA), and the strong coupling constant $\alpha_s(Q)$ was determined at different energy scales $Q = \sqrt{s}$. The results,

$$\alpha_s(22 \text{ GeV}) = 0.161_{-0.011}^{+0.016}, \quad \alpha_s(35 \text{ GeV}) = 0.143_{-0.007}^{+0.011}, \quad \alpha_s(44 \text{ GeV}) = 0.137_{-0.007}^{+0.010},$$

are in agreement with previous combined results of PETRA albeit with smaller uncertainties. Together with corresponding data from LEP, the energy dependence of α_s is significantly tested and is found to be in good agreement with the QCD expectation. Similarly, mean values of the observables were compared to analytic QCD predictions where hadronisation effects are absorbed in calculable power corrections.

⁽¹⁾ III. Physikalisches Institut der RWTH Aachen, D-52056 Aachen, Germany
contact e-mail: Otmar.Biebel@Physik.RWTH-Aachen.DE

⁽²⁾ CERN, European Organisation for Particle Physics, CH-1211 Geneva 23, Switzerland

⁽³⁾ for a full list of members of the JADE Collaboration see Reference [1]

1 Introduction

Summaries of measurements of α_s from various processes and at different energy scales Q demonstrate [2,3] that the energy dependence of $\alpha_s(Q)$ is in good agreement with the prediction of Quantum Chromodynamics (QCD). The uncertainties of these measurements, both experimental and theoretical, are different and their correlations are, in general, not known [2,3]. More quantitative studies of the running of α_s therefore require the existence of consistent measurements over large ranges of the energy scale Q , for the same process, using identical experimental techniques and theoretical calculations in order to minimise point-to-point systematic uncertainties.

Significant progress has been made in perturbative QCD calculations since 1992. Observables have been proposed for which perturbative predictions are extended beyond the next-to-leading-order ($\mathcal{O}(\alpha_s^2)$) [4], through the inclusion of leading and next-to-leading logarithms which are summed to all orders of α_s (NLLA) [5–7]. These calculations exhibit a better stability to contributions of unknown higher order corrections, which are usually estimated by variations of the renormalisation scale μ .

The experiments at LEP and SLC provided a number of significant determinations of α_s from hadronic event shapes and jet production, based on $\mathcal{O}(\alpha_s^2)$ +NLLA calculations, at centre-of-mass energies \sqrt{s} at and above 91 GeV, the mass of the Z^0 boson. Detailed studies of the high statistics data samples from the LEP experiments provide a better understanding of the phenomenology of the hadronisation process and thus of the modelling of hadronic final states with Monte Carlo programs. Determinations of α_s at LEP and SLC [8–12] therefore have smaller uncertainties than those which are available from previous measurements at lower e^+e^- centre-of-mass energies [1,13]. There are only a few recent measurements of α_s at lower energies. These either employed only some of the observables which are now available [14,15] or they were based on limited samples of Z^0 decays with final state photon radiation [16]. Therefore equivalent studies with data in the centre-of-mass energy range from $\sqrt{s} = 14$ to 46.7 GeV, taken at the PETRA collider which was shut down in 1986, are desirable.

In this paper we present an $\mathcal{O}(\alpha_s^2)$ +NLLA determination of α_s at $\sqrt{s} = 22, 35$, and 44 GeV using data from the JADE experiment [1,17] at PETRA. The selection of the JADE data and Monte Carlo event samples are described in Section 2. The measurement of event shape distributions, the corrections for detector imperfections and for initial state photon radiation as well as the estimate of the experimental uncertainties are outlined in Section 3. The corrected event shape distributions and the determination of the strong coupling constant $\alpha_s(Q)$ are presented in Section 4. A study of the energy dependence of mean values of event shape distributions and their comparison with analytic QCD calculations comprising power corrections to account for hadronisation effects is presented in Section 5. In Section 6 the results are summarised and the conclusions are drawn.

2 Data samples and Monte Carlo simulation

For the studies presented in this paper, we analysed data recorded with the JADE detector in 1981, 1984 to 1985, and 1986 at centre-of-mass energies of 22 GeV, 39.5–46.7 GeV, and

around 35 GeV, respectively. The JADE detector was one of the five experiments at the PETRA electron-positron collider. It was operated from 1979 until 1986 at centre-of-mass energies of $\sqrt{s} = 12$ to 46.7 GeV. A detailed description of the JADE detector can be found in [1, 17]. The main components of the detector were the central jet chamber to measure charged particle tracks and the lead glass calorimeter to measure energy depositions of electromagnetic showers, which both covered almost the whole solid angle of 4π .

Multihadronic events were selected by the standard JADE selection cuts [18] which were based on minimum energy deposits in the calorimeter and a minimum number of tracks emanating from the interaction region. All charged particle tracks with a total momentum of $|\vec{p}| > 100$ MeV/ c were considered in the analysis. Energy clusters in the electromagnetic calorimeter were considered if their energies exceeded 150 MeV after correction for energy deposited by associated tracks. Charged particle tracks were assumed to be pions while the photon hypothesis was assigned to electromagnetic energy clusters.

In order to remove background from two-photon processes and τ -pair events and from events which lost a substantial part of their energy due to hard initial state photon radiation, further constraints were imposed on the visible energy $E_{\text{vis}} = \sum E_i$, the total missing momentum $p_{\text{miss}} = |\sum \vec{p}_i|$ (\vec{p}_i and E_i are the 3-momentum and the energy of the tracks and clusters), the longitudinal balance relative to the e^+e^- beam axis of momenta $p_{\text{bal}} = |\sum p_i^z/E_{\text{vis}}|$ and the polar angle of the thrust axis, θ_T :

- $E_{\text{vis}} > \sqrt{s}/2$;
- $p_{\text{miss}} < 0.3 \cdot \sqrt{s}$;
- $p_{\text{bal}} < 0.4$;
- $|\cos \theta_T| < 0.8$.

With these cuts, the backgrounds from $\gamma\gamma$ and τ -pair events were reduced to less than 0.1% and 1%, respectively [19]. The final numbers of events which were retained for this analysis are listed in Table 1.

The retrieval of data files eleven years after shutdown of the experiment was difficult and turned out to be incomplete at this stage of the analysis. Comparisons of the numbers given in Table 1 with previous JADE publications [19–21] revealed that we were missing data sets of about 250 events around 22 GeV and about 450 events around 44 GeV. In addition, the original files containing information about the luminosity of different running periods could not be retrieved, so that only approximate values of integrated luminosities

year	\sqrt{s} [GeV]	data	MC
1981	22	1404	—
1984/85	40-48	6158	14 497
1986	35	20 926	25 123

Table 1: Number of events in data and in Monte Carlo detector simulation retained after application of the multihadron selection cuts described in the text.

\sqrt{s}	Ref. [19]	this analysis
22 GeV		
R_2	72.5 ± 1.2	72.7 ± 1.2
R_3	27.1 ± 1.2	27.0 ± 1.2
R_4	0.42 ± 0.16	0.28 ± 0.14
35 GeV		
R_2	77.7 ± 0.4	78.2 ± 0.3
R_3	22.0 ± 0.4	21.6 ± 0.3
R_4	0.31 ± 0.05	0.24 ± 0.03
44 GeV		
R_2	79.8 ± 0.5	79.2 ± 0.5
R_3	20.1 ± 0.5	20.7 ± 0.5
R_4	0.14 ± 0.05	0.15 ± 0.05

Table 2: A comparison of relative n -jet production rates R_n , as percentages of all hadronic events, using the JADE jet finding algorithm with $y_{\text{cut}} = 0.08$ [19]. No corrections are applied; the errors are statistical only.

corresponding to our final number of events can be given¹: the data samples shown in Tab. 1 correspond to about 2.4 pb^{-1} , 80 pb^{-1} and 40 pb^{-1} at 22 GeV, 35 GeV and 44 GeV centre-of-mass energy, respectively.

In order to verify the compatibility of this study with results which were previously published by JADE, we repeated a determination of the relative 2-, 3- and 4-jet event production rates as published in [19], using the original JADE jet finder with a resolution parameter of $y_{\text{cut}} = 0.08$. The results are presented in Table 2. Considering the fact that our present data samples at 22 GeV and 44 GeV lack about 10% of the original ones and that the samples around 35 GeV are from different running periods (1986 for this analysis, 1984-1985 for Reference [19]), the agreement between the old and this new study is very good. This demonstrates that we are able to perform detailed studies of event properties in a consistent way.

Corresponding Monte Carlo detector simulation data were retrieved for 35 and 44 GeV. They were generated using the QCD parton shower event generator JETSET 6.3 [22]. The Monte Carlo events at 35 GeV were generated using the coherent branching for the parton shower while the 44 GeV events had non-coherent branching². The main parameters used for event generation are given in Section 3.3. Both samples included a simulation of the acceptance and resolution of the JADE detector.

Comparisons of the measured and simulated distributions of visible energy, momentum balance, missing momentum and other quantities showed that the Monte Carlo simulation gave a reasonable description of the measurements. The simulated data can thus be

¹It is not expected that the missing events alter the measured distributions in a systematic manner. Also, detailed knowledge of luminosities is not required for the following studies of *normalised* event shape distributions.

²The different treatment of coherence in these samples of simulated data has no visible influence on the results of this study; see also Fig. 1, Figs. 3-5 and the discussions in Section 3.

used to correct for detector effects in the measured data. As an example we show in Figure 1 the distributions of the thrust observable $1 - T$ and of the differential two-jet rates D_2 , measured at 35 and at 44 GeV. The definitions of these observables are given in Section 3.1. In general, we found a good agreement of the detector simulation with data for all event shape distributions studied here, irrespective of coherent or non-coherent parton branching.

3 Experimental procedure

3.1 Event shapes and differential 2-jet rate

From the data samples described in the previous section, the event shape distributions of thrust, the heavy jet mass, the total and wide jet broadening and the differential 2-jet event rate using the Durham jet finder were determined. For convenience we list the definitions of these observables.

Thrust T :

The thrust value of a hadronic event is defined by the expression [23]

$$T = \max_{\vec{n}} \left(\frac{\sum_i |\vec{p}_i \cdot \vec{n}|}{\sum_i |\vec{p}_i|} \right) .$$

The vector \vec{n} which maximises the expression in parentheses is the thrust axis \vec{n}_T . It is used to divide an event into two hemispheres H_1 and H_2 by a plane through the origin and perpendicular to the thrust axis.

Heavy Jet Mass M_H :

From the particles in each of the two hemispheres defined by the thrust axis an invariant mass is calculated. The heavy jet mass M_H [24,25] is defined by the larger of the two masses. This analysis used the heavy jet mass scaled by the visible energy E_{vis} .

Jet Broadening B :

The jet broadening measures are calculated by the expression [5]:

$$B_k = \left(\frac{\sum_{i \in H_k} |\vec{p}_i \times \vec{n}_T|}{2 \sum_i |\vec{p}_i|} \right)$$

for each of the two hemispheres, H_k , defined above. The total jet broadening is given by $B_T = B_1 + B_2$. The wide jet broadening is defined by $B_W = \max(B_1, B_2)$.

Durham differential 2-jet rate D_2 :

Jets are reconstructed by a standard recombination algorithm: For any combination of two particles i and j in an event a measure of distance, y_{ij} , is calculated according to the Durham recombination scheme [26]

$$y_{ij} = \frac{2 \cdot \min(E_i^2, E_j^2) \cdot (1 - \cos \theta_{ij})}{E_{\text{vis}}^2} ,$$

where E_i and E_j are the energies of the particles and $\cos\theta_{ij}$ is the angle between their 3-momentum vectors. The pair i, j of particles with the smallest value of y_{ij} is replaced by a pseudoparticle k with 4-momentum $p_k = p_i + p_j$. This procedure is repeated until exactly three pseudoparticles remain which are called jets. The smallest y_{ij} corresponding to these three jets is indicated by y_{23} throughout the paper. At this particular value the number of reconstructed jets changes from 3 to 2. D_2 is the normalised differential cross-section as a function of y_{23} [27].

In the following we use the symbols T , M_H , B_T , B_W and D_2 to denote thrust, heavy jet mass, total and wide jet broadening, and the differential 2-jet rate, respectively.

3.2 Correction procedure

The event shape data were corrected for the limited acceptance and resolution of the detector and for initial state photon radiation effects by applying a bin-by-bin correction procedure. Correction factors were defined by the ratio of the distribution calculated from events generated by JETSET 6.3 at *hadron level* over the same distribution at *detector level*. The *hadron level* distributions were obtained from JETSET 6.3 generator runs without detector simulation and without initial state radiation, using all particles with lifetimes $\tau > 3 \cdot 10^{-10}$ s. The model events at *detector level* contained initial state photon radiation and a detailed simulation of the detector response and were processed in the same way as the data.

In a second step, the data distributions were further corrected for hadronisation effects. This was done by applying bin-by-bin correction factors derived from the ratio of the distribution at *parton level* over the same distribution at *hadron level*, which were calculated from JETSET generated events before and after hadronisation, respectively. The data distributions, thus corrected to the *parton level*, can be compared to analytic QCD calculations.

3.3 Systematic uncertainties

To study systematic uncertainties of the corrected data distributions we modified details of the event selection and of the correction procedure. For each variation the whole analysis was repeated and any deviation from the main result was considered a systematic error. In general, the maximum deviation from the main result for each kind of variation was regarded as symmetric systematic uncertainty. The main result was obtained using the default selection and correction procedure as described above.

We restricted the measurement of the event shape distributions to rely either on tracks or on clusters only. We varied the cut on $\cos\theta_T$ by ± 0.1 . The cut on p_{miss} was either removed or tightened to $p_{\text{miss}} < 0.25 \cdot \sqrt{s}$. Similarly, the momentum balance requirement was either restricted to $p_{\text{bal}} < 0.3$ or dropped. We also varied the cut for the visible energy E_{vis} by $\pm 0.05 \cdot \sqrt{s}$. In order to check the residual contributions from τ -pair events we also required at least seven well-measured charged tracks.

To study the impact of the hadronisation model of the JETSET 6.3 generator, the values of several significant model parameters were varied around their tuned default values used for our main result. We took the tuned values from Reference [21], where the

QCD parameter was $\Lambda_{\text{QCD}} = 400$ MeV, the cut-off for the parton shower development was $Q_0 = 1$ GeV, and the width of the transverse momentum distribution of the hadrons with respect to the direction of the quark was $\sigma_0 = 300$ MeV. According to this Reference we chose the LUND symmetric fragmentation function with $a = 0.5$ and $b = 0.9$ for the fragmentation of the light u, d, and s quarks. The heavy c and b quark were fragmented applying the Peterson et al. [28] fragmentation function using $\epsilon_c = 0.05$ and $\epsilon_b = 0.01$ [21].

Different sets of correction factors to correct the data from *hadron level* to *parton level* were generated by varying single parameters of the JETSET generator. The variations were chosen to be similar to the one standard deviation percentage limits obtained by the OPAL Collaboration from a parameter tuning of JETSET at $\sqrt{s} = M_{Z^0}$ [29].

In particular, we investigated the effects due to parton shower, hadronisation parameters, and quark masses. The amount of gluon radiation during the parton shower development was modified by varying Λ_{QCD} by ± 50 MeV. To vary the onset of hadronisation, we altered the parton shower cut-off parameter Q_0 by ± 0.5 GeV. We extrapolated the observed variation of α_s to reflect a variation of Q_0 between 0 and 2 GeV. The width of the transverse momentum distribution in the hadronisation process was varied by ± 30 MeV. The LUND symmetric fragmentation function was varied by changing the a parameter by ± 0.225 whereas the b parameter was kept fixed. As a systematic variation we used the LUND fragmentation function also for charm and bottom quarks. The effects due to the bottom quark mass were studied by restricting the model calculations which were used to determine the correction factors to up, down, strange, and charm quarks (udsc) only. In this case, any deviation from our main result was treated as asymmetric error.

No *detector level* Monte Carlo simulation data were available for the 22 GeV data. In order to obtain consistent detector corrections also at this energy, we studied the energy dependence of the detector correction from the 35 and 44 GeV Monte Carlo samples. Here we considered only the differential 2-jet rate, D_2 , of the Durham jet finder scheme because it is known to depend to a lesser extent on hadronisation and detector effects. In Figure 2 the detector correction factors as obtained at 35 GeV and at 44 GeV are displayed. In general, the corrections are small, and their size is about the same at both centre-of-mass energies. There is no apparent energy dependence of the detector correction within the range, indicated by the arrow, which was considered for the fit of α_s at 22 GeV. We therefore applied the 35 GeV detector correction to the differential 2-jet rate measured from the 22 GeV data, and studied only the well known dominating sources of systematic uncertainties. The correction of *hadronisation* effects was then determined from JETSET generator runs at 22 GeV centre-of-mass energies, exactly as for the data at 35 and 44 GeV.

4 Determination of α_s

4.1 Corrected event shape distributions

After applying the corrections for detector and for initial state radiation effects we obtained the event shape distributions at *hadron level*. These are shown in Figures 3, 4, and 5 for the 44, 35, and 22 GeV data samples. For comparison the respective distributions predicted by the JETSET 6.3 generator, at *hadron level*, are also shown. There is excellent agreement between the data and the model over the whole kinematic range of the

observables. In Tables 4, 5 and 6 the corrected data values are listed with statistical errors and experimental systematic uncertainties. The mean values of the distributions are also given.

4.2 QCD calculations for event shapes

The distributions of the event shape observables used in this analysis are predicted in perturbative QCD by a combination of the $\mathcal{O}(\alpha_s^2)$ [4] and the NLLA [5–7] calculations. The $\mathcal{O}(\alpha_s^2)$ calculation yields an expression of the form

$$R_{\mathcal{O}(\alpha_s^2)}(y) = 1 + A(y) \left(\frac{\alpha_s}{2\pi}\right) + B(y) \left(\frac{\alpha_s}{2\pi}\right)^2,$$

where $R(y) = \int_0^y dy' 1/\sigma_0 \cdot d\sigma/dy'$ is the cumulative cross-section of an event shape observable y normalised to the lowest order Born cross-section σ_0 . The NLLA calculations give an expression for $R(y)$ in the form:

$$R_{\text{NLLA}}(y) = \left(1 + C_1 \left(\frac{\alpha_s}{2\pi}\right) + C_2 \left(\frac{\alpha_s}{2\pi}\right)^2\right) \cdot \exp \left[L g_1 \left(\frac{\alpha_s}{2\pi} L\right) + g_2 \left(\frac{\alpha_s}{2\pi} L\right) \right]$$

where $L = \ln(1/y)$. The functions g_1 and g_2 are given by the NLLA calculations. The coefficients C_1 and C_2 are known from the $\mathcal{O}(\alpha_s^2)$ matrix elements.

4.3 Determination of α_s using $\mathcal{O}(\alpha_s^2)$ +NLLA calculations

We determined α_s by χ^2 fits to event shape distributions of $1 - T$, M_H , B_T , B_W and of D_2 corrected to the *parton level*. For the sake of direct comparison to other published results we closely followed the procedures described in [11, 30, 31]. We chose the so-called $\ln(R)$ -matching scheme to merge the $\mathcal{O}(\alpha_s^2)$ with the NLLA calculations. The renormalisation scale factor, $x_\mu \equiv \mu/\sqrt{s}$, was set to $x_\mu = 1$ for what we chose to be the main result. Here, the value of μ defines the energy scale at which the theory is renormalised.

The fit ranges for each observable were determined by choosing the largest range for which the hadronisation uncertainties remained small, for which the $\chi^2/\text{d.o.f.}$ of the fits did not significantly exceed unity, and by requiring reasonably stable fits under changes of the range. The remaining variations of the fit results due to the choice of fit range were taken as systematic uncertainties. The finally selected fit ranges, the results of the χ^2 fits and of the study of systematic uncertainties are tabulated in Tables 7, 8, and 9 and are shown in Figures 6, 7, and 8.

The dependence of the fit result for α_s on x_μ indicates the importance of higher order terms in the theory. We also changed the renormalisation scale factor in the range of $x_\mu = 0.5$ to 2.0. We found variations of similar size as the uncertainties from the detector correction and the hadronisation model dependence. The differential 2-jet rate, D_2 , in the Durham jet scheme exhibits the smallest experimental and renormalisation scale uncertainties, resulting in the smallest total error of all observables considered in this analysis. The values of α_s and the errors obtained at 35 and 44 GeV are shown in Figure 9. In these diagrams also the α_s values measured by the OPAL Collaboration at $\sqrt{s} = M_{Z^0}$ [11]

are shown for comparison. The values of α_s exhibit a similar scattering pattern at all energies. This demonstrates the strong correlation of the systematic uncertainties, which are dominated by theoretical and hadronisation uncertainties.

The individual results of the four event shape observables and the differential 2-jet rate were combined into a single value following the procedure described in References [11, 30, 32]. At each energy, a weighted average of the five α_s values was calculated with the reciprocal of the square of the respective total error used as a weight. In the case of asymmetric errors we took the average of the positive and negative error to determine the weight. For each of the systematic checks, the mean of the α_s values from all considered observables was determined. Any deviation of this mean from the weighted average of the main result was taken as a systematic uncertainty.

With this procedure we obtained as final results for α_s

$$\begin{aligned}\alpha_s(44 \text{ GeV}) &= 0.1372 \pm 0.0017(\text{stat.}) \begin{matrix} +0.0101 \\ -0.0069 \end{matrix}(\text{syst.}) \\ \alpha_s(35 \text{ GeV}) &= 0.1434 \pm 0.0010(\text{stat.}) \begin{matrix} +0.0112 \\ -0.0065 \end{matrix}(\text{syst.}) \\ \alpha_s(22 \text{ GeV}) &= 0.1608 \pm 0.0083(\text{stat.}) \begin{matrix} +0.0137 \\ -0.0058 \end{matrix}(\text{syst.}) ,\end{aligned}$$

where the result at 22 GeV is based on the differential 2-jet rate only. The systematic errors at 44, 35, and 22 GeV are the quadratic sums of the experimental uncertainties (± 0.0034 , ± 0.0018 , ± 0.0030), the effects due to the Monte Carlo modelling ($\begin{matrix} +0.0049 & +0.0068 & +0.0116 \\ -0.0027 & -0.0034 & -0.0050 \end{matrix}$) and the contributions due to the variation of the renormalisation scale ($\begin{matrix} +0.0082 & +0.0087 \\ -0.0054 & -0.0052, \\ +0.0066 \\ -0.0001 \end{matrix}$). It should be noted that the modelling uncertainties due to quark mass effects contribute significantly to the total error.

4.4 Determination of α_s using $\mathcal{O}(\alpha_s^2)$ calculations

For comparison, we repeated the α_s fits using fixed order $\mathcal{O}(\alpha_s^2)$ calculations only. The fit ranges for each distribution had to be readjusted in order to match the stability requirements given above³. All systematic checks were done as described above except for the variation of the renormalisation scale factor x_μ . Instead, the $\mathcal{O}(\alpha_s^2)$ -fits were performed once with x_μ fixed to 1 and once with x_μ as a free parameter of the fit. The mean value of α_s from the two fits was taken as the final result while half of the difference between the two was assigned as a systematic error due to the unknown higher orders in perturbation theory. The results of the $\mathcal{O}(\alpha_s^2)$ fits are summarised in Tables 10 and 11. The corresponding theoretical predictions were superimposed on the results of the $\mathcal{O}(\alpha_s^2)$ +NLLA fits that are presented in Figures 6 and 7. All results at a given centre-of-mass energy agree with each other but the α_s values from the $\mathcal{O}(\alpha_s^2)$ +NLLA fits are systematically lower. Again, the pattern between these results and those obtained at the higher energies of LEP [32] is very similar.

³From corresponding studies at LEP [11, 32] it is known that different fit ranges are required for the $\mathcal{O}(\alpha_s^2)$ and for $\mathcal{O}(\alpha_s^2)$ +NLLA predictions. This is also supported by theoretical considerations, since the inclusion of NLLA is supposed to extend the degree of reliability especially in the 2-jet region of phase space, i.e. at small values of the event shape observables used in this study.

5 Mean Values of Distributions and QCD Power Corrections

5.1 Power corrections

The value of α_s can also be assessed by the energy dependence of mean values of event shape distributions. Presently, the mean values of the observables considered in this analysis are calculated up to $\mathcal{O}(\alpha_s^2)$. For an observable \mathcal{F} the perturbative prediction is

$$\langle \mathcal{F}^{\text{pert.}} \rangle = A_{\mathcal{F}} \left(\frac{\alpha_s}{2\pi} \right) + (B_{\mathcal{F}} - 2A_{\mathcal{F}}) \left(\frac{\alpha_s}{2\pi} \right)^2$$

where the coefficients $A_{\mathcal{F}}$ and $B_{\mathcal{F}}$ were determined from the $\mathcal{O}(\alpha_s^2)$ perturbative calculations [4, 5, 25, 33]. The term $-2A_{\mathcal{F}}$ accounts for the difference between the total cross-section used in the measurement and the Born level cross-section used in the perturbative calculation. The numerical values of these coefficients are summarised in Table 3.

Instead of correcting for hadronisation effects with a Monte Carlo event generator as we did for the α_s determination presented in Section 4, we considered additive power-suppressed corrections ($1/(\sqrt{s})^p$) to the perturbative predictions of the mean values of the event shape observables. Such corrections are expected on general grounds for hadronisation and other non-perturbative effects, for example renormalons [35]. The non-perturbative effects are due to the emission of very low energetic gluons which can not be treated perturbatively due to the divergence of the perturbative expressions for α_s at low scales. In the calculations of Reference [34] which we used in this analysis a non-perturbative parameter

$$\bar{\alpha}_p(\mu_I) = \frac{p+1}{\mu_I^{p+1}} \int_0^{\mu_I} dk \alpha_s(k) \cdot k^p$$

was introduced to replace the divergent portion of the perturbative expression for $\alpha_s(\sqrt{s})$ below an infrared matching scale μ_I . The general form of the power correction to the mean value of an observable \mathcal{F} assumes the form

$$\begin{aligned} \langle \mathcal{F}^{\text{pow.}} \rangle &= a_{\mathcal{F}} \frac{4C_F}{\pi p} \cdot \left(\frac{\mu_I}{\sqrt{s}} \right)^p \cdot \ln^r \left(\frac{\sqrt{s}}{\mu_I} \right) \\ &\cdot \left[\bar{\alpha}_{p-1}(\mu_I) - \alpha_s(\sqrt{s}) - \frac{\beta_0}{2\pi} \left(\ln \frac{\sqrt{s}}{\mu_I} + \frac{K}{\beta_0} + \frac{1}{p} \right) \alpha_s^2(\sqrt{s}) \right], \end{aligned}$$

Observable \mathcal{F}	$A_{\mathcal{F}}$	$B_{\mathcal{F}}$	$a_{\mathcal{F}}$	p	r
$\langle T \rangle$	2.103	44.99	-1	1	0
$\langle M_H^2/s \rangle$	2.103	23.24	1.0 ± 0.5	1	0
$\langle B_T \rangle$	4.066	64.24	1.0 ± 0.5	1	1
$\langle B_W \rangle$	4.066	-9.53	1.0 ± 0.5	1	1
$\langle y_{23} \rangle$	0.895	12.68	—	2	—

Table 3: Coefficients of the perturbative prediction [4, 5, 25, 33] and coefficients and parameters of the power corrections [34] to the mean values of the event shape observables.

where $C_F = 4/3$. The factor $\beta_0 = (11C_A - 2N_f)/3$ stems from the QCD β -function of the renormalisation group equation. It depends on the number of colours, $C_A = 3$, and number of active quark flavours N_f , for which we used $N_f = 5$ throughout the analysis. The term $K = (67/18 - \pi^2/6)C_A - 5/9 \cdot N_f$ originates from the choice of the $\overline{\text{MS}}$ renormalisation scheme. The remaining coefficient $a_{\mathcal{F}}$ and the parameters p and r depend on the event shape observable. For completeness, these coefficients and parameters obtained in Reference [34] are also listed in Table 3.

5.2 Determination of α_s using power corrections

We determined $\alpha_s(M_{Z^0})$ by χ^2 fits of the expression

$$\langle \mathcal{F} \rangle = \langle \mathcal{F}^{\text{pert.}} \rangle + \langle \mathcal{F}^{\text{pow.}} \rangle.$$

to the mean values of the five observables investigated in this analysis including the measured mean values obtained by other experiments at different centre-of-mass energies [10, 31, 36, 37]. For the central values of α_s from the fits we chose a renormalisation scale factor of $x_\mu = 1$ and an infrared scale of $\mu_I = 2$ GeV. The $\chi^2/\text{d.o.f.}$ of all fits were between 0.8 ($\langle M_H^2/s \rangle$) and 4.2 ($\langle B_T \rangle$). We estimated the systematic uncertainties by varying x_μ from 0.5 to 2 and μ_I from 1 to 3 GeV. Since the precision of the coefficient $a_{\mathcal{F}}$ as given in Reference [34] for the heavy jet mass M_H and the two jet broadening measures, B_T and B_W is only $\pm 50\%$, we assigned an additional uncertainty to α_s due to the variation of these coefficients by this amount.

In the case of $\langle y_{23} \rangle$ no coefficient $a_{\mathcal{F}}$ is given in Reference [34]. We investigated the size of $a_{\mathcal{F}}$ by fitting with α_s fixed to the world average [2, 3] $\alpha_s^{\text{w.a.}}(M_{Z^0}) = 0.118$. All fits with $p = 1$ or 2, and $r = 0$ or 1 resulted in very small values of $a_{\mathcal{F}}$ compatible with zero. From this we conclude that power corrections to the perturbative prediction for $\langle y_{23} \rangle$ can be neglected for the energy range considered. Therefore, we used the perturbative prediction only, for which we obtained a good fit with $\chi^2/\text{d.o.f.} = 1$.

The results of the fits are shown in Figure 10 and the numeric values are listed in Table 12. It presents the values for α_s and for $\bar{\alpha}_0$, the experimental errors and systematic uncertainties of the fit results.

Employing the procedure used in Section 4 to combine the individual α_s values, we obtained

$$\alpha_s(M_{Z^0}) = 0.1155^{+0.0062}_{-0.0045}$$

where the error is the experimental uncertainty (± 0.0013), the renormalisation scale uncertainty ($^{+0.0045}_{-0.0033}$), the uncertainty due to the choice of the infrared scale ($^{+0.0029}_{-0.0019}$) and the uncertainties of the non-perturbative coefficients $a_{\mathcal{F}}$ ($^{+0.0028}_{-0.0020}$), all combined in quadrature. This result is in good agreement with the world average value [2] of $\alpha_s^{\text{w.a.}}(M_{Z^0}) = 0.118 \pm 0.006$. Our value is also in agreement with the results of similar studies for different sets of observables by the DELPHI Collaboration [37] and by the H1 Collaboration [38].

6 Summary and Conclusions

Data recorded by the JADE experiment at centre-of-mass energies around 22, 35, and 44 GeV were analysed in terms of event shape distributions and differential 2-jet rates. For most of the observables no experimental results have previously been presented, because the total and wide jet broadening, B_T and B_W , as well as the Durham jet finding scheme were proposed only after the shutdown of the experiments at the PETRA accelerator.

The measured distributions were corrected for detector and initial state photon radiation effects using original Monte Carlo simulation data for 35 and 44 GeV. The simulated data are based on the JETSET parton shower generator version 6.3. The same event generator was also employed to correct the data for hadronisation effects in order to determine the strong coupling constant α_s .

Our measurements of α_s are based on the most complete theoretical calculations available to date. For all observables theoretical calculations exist in $\mathcal{O}(\alpha_s^2)$ and in the next-to-leading log approximation. These two calculations were combined using the $\ln(R)$ -matching scheme.

The final values of α_s at the three different centre-of-mass energies are

$$\begin{aligned}\alpha_s(44 \text{ GeV}) &= 0.137^{+0.010}_{-0.007} \\ \alpha_s(35 \text{ GeV}) &= 0.143^{+0.011}_{-0.007} \\ \alpha_s(22 \text{ GeV}) &= 0.161^{+0.016}_{-0.011},\end{aligned}$$

where the errors are statistical, experimental systematics, Monte Carlo modelling and higher order QCD uncertainties added in quadrature. The dominant contributions to the total error came from the choice of the renormalisation scale and from uncertainties due to quark mass effects.

The α_s result at 22 GeV was obtained from the differential 2-jet rate only. Note, however, that for 35 and 44 GeV the α_s value obtained from the differential 2-jet rate is very close to the weighted average as can be inferred from Figure 9. We therefore consider the α_s value measured at 22 GeV a good estimate of the weighted average at this energy.

The fits for α_s were also performed using the $\mathcal{O}(\alpha_s^2)$ calculation alone. All results were found to be consistent with each other.

These results agree well with those which are available from previous measurements of α_s in the PETRA and PEP energy range; see e.g. [1, 13] for reviews of that time. Our results, however, include more detailed systematic studies, are based on more observables and use more advanced theoretical calculations; nevertheless they exhibit smaller total errors.

Similarities between the main components of the JADE detector [17] at PETRA and the OPAL detector [39] at LEP, as well as between this analysis and studies performed by the OPAL Collaboration [11, 30, 31] at $\sqrt{s} = 91.2, 133,$ and 161 GeV, suggest the energy dependence of α_s in the centre-of-mass energy range of $\sqrt{s} = 22\text{-}161$ GeV can be reliably tested, because the systematic uncertainties of these measurements are partly correlated.

The α_s results from OPAL and from this analysis are shown in Figure 11. The result of a χ^2 fit of the $\mathcal{O}(\alpha_s^3)$ QCD prediction [40] to the data is shown by the solid line. The

fit resulted in $\alpha_s(M_{Z^0}) = 0.1207 \pm 0.0012$ ⁴ and $\chi^2/\text{d.o.f.} = 4.9/5$, taking into account only statistical and experimental uncertainties, which are displayed in Fig. 11 as the solid, innermost error bars. The other systematic uncertainties, due to hadronisation and to unknown higher order contributions, are assumed to be fully correlated at all energies and thus are not considered in this test of the *energy dependence* of α_s . A visible trend of the lower energy results all lying above and the higher energy ones lying below the fitted QCD curve can be consistently explained within the assigned experimental uncertainties which is indicated by the value of $\chi^2/\text{d.o.f.} = 1$.

A χ^2 fit for the hypothesis of a constant value of α_s gives $\alpha_s = 0.1328 \pm 0.0014$ and $\chi^2/\text{d.o.f.} = 101/5$, which has a vanishing probability. The energy dependence of α_s is therefore significantly demonstrated by the results from the combined JADE and OPAL data.

Evolving our α_s measurements to $\sqrt{s} = M_{Z^0}$ the results obtained at 44, 35 and 22 GeV transform to $0.122^{+0.008}_{-0.006}$, $0.122^{+0.008}_{-0.006}$, and $0.124^{+0.009}_{-0.007}$, respectively. The combination of these values gives $\alpha_s(M_{Z^0}) = 0.122^{+0.008}_{-0.005}$. This value is consistent with the direct measurement at $\sqrt{s} = M_{Z^0}$ by the OPAL Collaboration of $\alpha_s(M_{Z^0}) = 0.117^{+0.008}_{-0.006}$ [11], for the same subset of observables.

The energy dependence of the mean values of the distributions can be directly compared with analytic QCD predictions plus power corrections for hadronisation effects [34]. Until recently, such studies were hardly possible since for most of the observables no results were available at energies below the Z^0 mass scale. With the inclusion of the results presented in this paper, comprehensive fits of the analytic predictions to the data are now possible. Our studies resulted in

$$\alpha_s(M_{Z^0}) = 0.116^{+0.006}_{-0.005}$$

which is in good agreement with our results from the $\mathcal{O}(\alpha_s^2)$ +NLLA fits, with measurements at LEP [37] and at HERA [38] and also with the world average value.

In summary, new studies of hadronic final states of e^+e^- -annihilations in the PETRA energy range provided valuable information which was not available before. New results of α_s , obtained in a similar manner as those from the experiments at LEP, provide a significant test of the running of α_s and thus of the non-abelian nature of QCD. Evolved to the Z^0 mass scale, the results are in good agreement with those obtained at LEP, and are of similar precision. A direct comparison of the energy dependence of the mean values of the measured distributions with analytic QCD calculations plus power corrections provide alternative ways to test QCD, without the need to rely on phenomenological hadronisation models.

Work has been started to further decrease the overall uncertainties of the results presented in this paper, and to study more aspects of QCD using the JADE data samples. This can be achieved by the use of more recent event generators and the JADE detector simulation software. This will provide the possibility to study the data at the lowest PETRA energies, around $\sqrt{s} = 14$ and 22 GeV, in more detail, i.e. for energy scales at which the variation of α_s is strongest. In addition, the significance of results from data at PETRA energies will increase from a better and more fundamental treatment of the b-quark mass, in theory [41] as well as in experiment. Together with the most recent data

⁴This value of $\alpha_s(M_{Z^0})$ corresponds to a QCD scale $\Lambda_{\overline{\text{MS}}}^{(5)} = 242 \pm 15$ MeV for five active quark flavours.

of the LEP experiments, consistent studies of QCD properties and the running of α_s in the energy range of 14 up to over 180 GeV have the potential to reach a level of precision which was never available before.

Acknowledgements

We are grateful to the members of the former JADE Collaboration for providing the possibility to further analyse their data. We thank the DESY computer centre for copying old IBM format tapes to modern data storage devices before the shutdown of the DESY-IBM. We are especially indebted to G. Eckerlin, E. Elsen and J. Olsson for their valuable help to recover the data files and for numerous suggestions and comments on the analysis and on this manuscript. We thank R. Barlow for proof reading this manuscript. We also acknowledge the effort of J. von Krogh, P. Bock and many other colleagues to search for files and tapes containing JADE software, data and Monte Carlo simulation. S.K. and O.B. are also grateful to S. Catani and M.H. Seymour for providing the program EVENT2.

References

- [1] B. Naroska: *e^+e^- Physics with the JADE Detector at PETRA*, Phys. Rep. 148 (1987) 67.
- [2] S. Bethke: proceedings of the *QCD Euroconference 96*, Montpellier, France, July 4-12 (1996), Nucl. Phys. (Proc.Suppl.) 54A (1997) 314-326; hep-ex/9609014.
- [3] M. Schmelling: proceedings of the *XXVIII International Conference on High Energy Physics*, Warsaw, Poland, July 25-31 (1996), Edited by Z. Ajduk and A.K. Wroblewski, World Scientific, 1997; hep-ex/9701002.
- [4] R.K. Ellis, D.A. Ross, A.E. Terrano: Nucl. Phys. **B178** (1981) 421.
- [5] S. Catani, G. Turnock, B.R. Webber: Phys. Lett. **B295** (1992) 269.
- [6] S. Catani, L. Trentadue, G. Turnock and B.R. Webber: Nucl. Phys. **B407** (1993) 3.
- [7] G. Dissertori, M. Schmelling: Phys. Lett. **B361** (1995) 167.
- [8] ALEPH Coll., D. Decamp et al.: Phys. Lett. **B284** (1992) 408.
- [9] DELPHI Coll., P. Abreu et al.: Z. Phys. **C59** (1993) 21.
- [10] L3 Coll., M. Acciarri et al.: Phys. Lett. **B404** (1997) 390.
- [11] OPAL Coll., P.D. Acton et al.: Z. Phys. **C59** (1993) 1.
- [12] SLD Coll., K. Abe et al.: Phys. Rev **D51** (1995) 962.
- [13] S. Bethke: proceedings of the *Workshop on the Standard Model at Present and Future Accelerator Energies*, Budapest, Hungary, 1989, ed. F. Csikor, G. Pocsik, E. Toth, Nova Science, 1992; LBL-28112 (1989).
- [14] TPC/ 2γ Coll., D.A. Bauer et al.: SLAC-PUB-6518, 1994.
- [15] TOPAZ Coll., Y. Ohnishi et al.: Phys. Lett. **B313** (1993) 475;
TOPAZ Coll., M. Aoki et al.: GLS-0944, paper submitted to the *XXVII International Conference on High Energy Physics*, Glasgow, July 20-27 (1994).
- [16] L3 Coll., M. Acciarri et al.: CERN-PPE/97-74 (June 1997), submitted to Phys. Lett. **B**.
- [17] JADE Coll., W. Bartel et al.: Phys. Lett. **88B** (1979) 171.
- [18] JADE Coll., W. Bartel et al.: Phys. Lett. **129B** (1983) 145.
- [19] JADE Coll., S. Bethke et al.: Phys. Lett. **B213** (1988) 235.
- [20] JADE Coll., W. Bartel et al.: Z. Phys. **C33** (1986) 23.
- [21] JADE Coll., E. Elsen et al.: Z. Phys. **C46** (1990) 349.

- [22] T. Sjöstrand: *Comput. Phys. Commun.* **39** (1986) 347;
T. Sjöstrand, M. Bengtsson: *Comput. Phys. Commun.* **43** (1987) 367.
- [23] S. Brandt et al.: *Phys. Lett.* **B12** (1964) 57;
E. Fahri: *Phys. Rev. Lett.* **39** (1977) 1587.
- [24] T. Chandramohan, L. Clavelli: *Nucl. Phys.* **B184** (1981) 365;
L. Clavelli, D. Wyler: *Phys. Lett.* **B103** (1981) 383.
- [25] Z. Kunszt, P. Nason, G. Marchesini, B.R. Webber: in *Z Physics at LEP 1*, vol. 1, ed. G. Altarelli, R. Kleiss and C. Verzegnassi, CERN Yellow Book 89-08.
- [26] S. Catani et al.: *Phys. Lett.* **B269** (1991) 432.
- [27] OPAL Coll., M.Z. Akrawy et al.: *Phys. Lett.* **B235** (1990) 389;
MARK-II Coll., S. Komamiya et al.: *Phys. Rev. Lett.* **64** (1990) 987.
- [28] C. Peterson, D. Schlatter, I. Schmitt, P.M. Zerwas: *Phys. Rev. D* **27** (1983) 105.
- [29] OPAL Coll., G. Alexander et al.: *Z. Phys.* **C69** (1995) 543.
- [30] OPAL Coll., G. Alexander et al.: *Z. Phys.* **C72** (1996) 191.
- [31] OPAL Coll., K. Ackerstaff et al.: *Z. Phys.* **C75** (1997) 193.
- [32] OPAL Coll., P.D. Acton et al.: *Z. Phys.* **C55** (1992) 1.
- [33] We used the program EVENT2 of S. Catani and M.H. Seymour to determine the perturbative coefficients by integrating the ERT $\mathcal{O}(\alpha_s^2)$ matrix elements [4]:
S. Catani, M.H. Seymour: *Phys. Lett.* **B378** (1996) 287.
- [34] Yu.L. Dokshitzer, B.R. Webber: *Phys. Lett.* **B352** (1995) 451;
B.R. Webber: proceedings of the *Workshop on Deep Inelastic Scattering and QCD (DIS 95)*, Paris, France, 24-28 Apr, 1995, ed. J.F. Laporte and Y. Sirois; Cavendish-HEP-95/11; hep-ph/9510283.
- [35] A.H. Mueller: in *QCD — 20 Years Later*, vol. 1, ed. P.M. Zerwas and H.A. Kastrup, World Scientific, Singapore, 1993.
- [36] ALEPH Coll., D. Buskulic et al.: *Z. Phys.* **C55** (1992) 209;
ALEPH Coll., D. Buskulic et al.: *Z. Phys.* **C73** (1997) 409;
AMY Coll., Y.K. Li et al.: *Phys. Rev.* **D41** (1990) 2675;
DELCO Coll., M. Sakuda et al.: *Phys. Rev.* **152B** (1985) 399;
DELPHI Coll., P. Abreu et al.: *Z. Phys.* **C73** (1996) 11;
L3 Coll., B. Adeva et al.: *Z. Phys.* **C55** (1992) 39;
L3 Coll., M. Acciarri et al.: *Phys. Lett.* **B371** (1996) 137;
MarkII Coll., A. Peterson et al.: *Phys. Rev.* **D37** (1988) 1;
MarkJ Coll., D.P. Barber et al.: *Phys. Rev. Lett.* **43** (1979) 901;
MarkJ Coll., D.P. Barber et al.: *Phys. Lett.* **85B** (1979) 463;

- OPAL Coll., P.D. Acton et al.: Z. Phys. **C55** (1992) 1;
OPAL Coll., G. Alexander et al.: Z. Phys. **C72** (1996) 191;
SLD Coll., K. Abe et al.: Phys. Rev. **D51** (1995) 962;
TASSO Coll., W. Braunschweig et al.: Z. Phys. **C41** (1988) 359;
TASSO Coll., W. Braunschweig et al.: Z. Phys. **C47** (1990) 187.
- [37] DELPHI Coll., P. Abreu et al.: Z. Phys. **C73** (1997) 229.
- [38] H1 Coll., C. Adloff et al.: Phys. Lett. **B406** (1997) 256.
- [39] OPAL Coll., K. Ahmet et al.: Nucl. Inst. Meth. A305 (1991) 275.
- [40] Particle Data Group, R.M. Barnett et al.: Phys. Rev. **D54** (1996) 1.
- [41] M. Bilenky, G. Rodrigo, A. Santamaria: Nucl. Phys. **B439** (1995) 505;
W. Bernreuther, A. Brandenburg, P. Uwer: Phys. Rev. Lett. **79** (1997) 189;
G. Rodrigo, A. Santamaria, M. Bilenky: Phys. Rev. Lett. **79** (1997) 193.

Tables

$1 - T$	$1/\sigma \cdot d\sigma/d(1 - T)$	M_H/\sqrt{s}	$1/\sigma \cdot d\sigma/d(M_H/\sqrt{s})$
0.00-0.02	$0.989 \pm 0.061 \pm 0.192$	0.00-0.06	$0.002 \pm 0.000 \pm 0.003$
0.02-0.04	$8.73 \pm 0.26 \pm 0.89$	0.06-0.10	$0.022 \pm 0.002 \pm 0.007$
0.04-0.06	$12.85 \pm 0.35 \pm 0.92$	0.10-0.14	$0.576 \pm 0.025 \pm 0.077$
0.06-0.08	$8.58 \pm 0.28 \pm 0.84$	0.14-0.18	$4.06 \pm 0.11 \pm 0.37$
0.08-0.10	$4.97 \pm 0.20 \pm 0.18$	0.18-0.22	$6.94 \pm 0.19 \pm 0.29$
0.10-0.12	$3.84 \pm 0.18 \pm 0.33$	0.22-0.26	$5.00 \pm 0.16 \pm 0.20$
0.12-0.14	$2.54 \pm 0.14 \pm 0.17$	0.26-0.30	$3.30 \pm 0.13 \pm 0.23$
0.14-0.16	$1.88 \pm 0.12 \pm 0.23$	0.30-0.34	$2.146 \pm 0.096 \pm 0.116$
0.16-0.18	$1.47 \pm 0.10 \pm 0.18$	0.34-0.38	$1.222 \pm 0.074 \pm 0.228$
0.18-0.20	$1.141 \pm 0.091 \pm 0.104$	0.38-0.42	$0.936 \pm 0.065 \pm 0.101$
0.20-0.23	$0.808 \pm 0.062 \pm 0.139$	0.42-0.46	$0.567 \pm 0.048 \pm 0.153$
0.23-0.26	$0.486 \pm 0.047 \pm 0.066$	0.46-0.50	$0.376 \pm 0.042 \pm 0.097$
0.26-0.30	$0.326 \pm 0.035 \pm 0.047$	0.50-0.55	$0.118 \pm 0.019 \pm 0.020$
0.30-0.35	$0.239 \pm 0.027 \pm 0.036$	0.55-0.60	$0.015 \pm 0.005 \pm 0.005$
0.35-0.40	$0.047 \pm 0.012 \pm 0.019$	mean value	$0.2470 \pm 0.0010 \pm 0.0008$
0.40-0.50	$0.001 \pm 0.001 \pm 0.002$		
mean value	$0.0860 \pm 0.0008 \pm 0.0011$		

B_T	$1/\sigma \cdot d\sigma/dB_T$	B_W	$1/\sigma \cdot d\sigma/dB_W$
0.00-0.03	$0.012 \pm 0.002 \pm 0.010$	0.00-0.02	$0.034 \pm 0.006 \pm 0.032$
0.03-0.06	$0.637 \pm 0.041 \pm 0.137$	0.02-0.04	$3.06 \pm 0.14 \pm 0.44$
0.06-0.08	$5.76 \pm 0.22 \pm 1.00$	0.04-0.06	$13.94 \pm 0.37 \pm 0.78$
0.08-0.10	$9.39 \pm 0.30 \pm 0.31$	0.06-0.08	$12.56 \pm 0.34 \pm 0.37$
0.10-0.12	$8.44 \pm 0.28 \pm 0.94$	0.08-0.10	$6.88 \pm 0.23 \pm 0.46$
0.12-0.14	$7.17 \pm 0.26 \pm 0.39$	0.10-0.12	$4.62 \pm 0.18 \pm 0.40$
0.14-0.16	$5.31 \pm 0.21 \pm 0.27$	0.12-0.14	$3.27 \pm 0.15 \pm 0.30$
0.16-0.18	$3.55 \pm 0.16 \pm 0.18$	0.14-0.16	$1.95 \pm 0.12 \pm 0.26$
0.18-0.20	$2.84 \pm 0.15 \pm 0.16$	0.16-0.18	$1.367 \pm 0.096 \pm 0.194$
0.20-0.22	$2.01 \pm 0.12 \pm 0.12$	0.18-0.20	$1.038 \pm 0.084 \pm 0.108$
0.22-0.24	$1.65 \pm 0.11 \pm 0.15$	0.20-0.23	$0.605 \pm 0.052 \pm 0.032$
0.24-0.27	$0.998 \pm 0.065 \pm 0.139$	0.23-0.26	$0.261 \pm 0.037 \pm 0.055$
0.27-0.30	$0.563 \pm 0.049 \pm 0.071$	0.26-0.30	$0.020 \pm 0.005 \pm 0.007$
0.30-0.35	$0.253 \pm 0.024 \pm 0.043$	mean value	$0.0848 \pm 0.0006 \pm 0.0004$
0.35-0.40	$0.018 \pm 0.006 \pm 0.013$		
mean value	$0.1344 \pm 0.0007 \pm 0.0015$		

Table 4: Event shape data at $\sqrt{s} = 44$ GeV for the observables described in the text. The values were corrected for detector and for initial state radiation effects. The first errors denote the statistical and the second the experimental systematic uncertainties.

$1 - T$	$1/\sigma \cdot d\sigma/d(1 - T)$	M_H/\sqrt{s}	$1/\sigma \cdot d\sigma/d(M_H/\sqrt{s})$
0.00-0.02	$0.638 \pm 0.028 \pm 0.181$	0.00-0.06	$0.002 \pm 0.000 \pm 0.004$
0.02-0.04	$6.43 \pm 0.12 \pm 0.23$	0.06-0.10	$0.017 \pm 0.001 \pm 0.009$
0.04-0.06	$11.00 \pm 0.17 \pm 0.25$	0.10-0.14	$0.288 \pm 0.009 \pm 0.041$
0.06-0.08	$9.47 \pm 0.16 \pm 0.43$	0.14-0.18	$2.566 \pm 0.043 \pm 0.095$
0.08-0.10	$6.43 \pm 0.13 \pm 0.21$	0.18-0.22	$6.278 \pm 0.090 \pm 0.361$
0.10-0.12	$4.049 \pm 0.095 \pm 0.173$	0.22-0.26	$5.463 \pm 0.088 \pm 0.319$
0.12-0.14	$3.033 \pm 0.084 \pm 0.239$	0.26-0.30	$3.823 \pm 0.073 \pm 0.173$
0.14-0.16	$1.962 \pm 0.065 \pm 0.151$	0.30-0.34	$2.390 \pm 0.056 \pm 0.084$
0.16-0.18	$1.704 \pm 0.062 \pm 0.179$	0.34-0.38	$1.643 \pm 0.047 \pm 0.088$
0.18-0.20	$1.209 \pm 0.050 \pm 0.117$	0.38-0.42	$1.008 \pm 0.037 \pm 0.039$
0.20-0.23	$0.922 \pm 0.036 \pm 0.066$	0.42-0.46	$0.626 \pm 0.030 \pm 0.040$
0.23-0.26	$0.754 \pm 0.035 \pm 0.095$	0.46-0.50	$0.427 \pm 0.025 \pm 0.067$
0.26-0.30	$0.453 \pm 0.022 \pm 0.049$	0.50-0.55	$0.153 \pm 0.013 \pm 0.034$
0.30-0.35	$0.186 \pm 0.012 \pm 0.061$	0.55-0.60	$0.020 \pm 0.004 \pm 0.005$
0.35-0.40	$0.070 \pm 0.008 \pm 0.010$	mean value	$0.2601 \pm 0.0006 \pm 0.0016$
0.40-0.50	$0.001 \pm 0.001 \pm 0.001$		
mean value	$0.0938 \pm 0.0004 \pm 0.0015$		

B_T	$1/\sigma \cdot d\sigma/dB_T$	B_W	$1/\sigma \cdot d\sigma/dB_W$
0.00-0.03	$0.018 \pm 0.003 \pm 0.028$	0.00-0.02	$0.041 \pm 0.006 \pm 0.046$
0.03-0.06	$0.381 \pm 0.019 \pm 0.103$	0.02-0.04	$1.628 \pm 0.059 \pm 0.276$
0.06-0.08	$3.371 \pm 0.089 \pm 0.279$	0.04-0.06	$11.79 \pm 0.18 \pm 0.46$
0.08-0.10	$8.02 \pm 0.15 \pm 0.82$	0.06-0.08	$12.18 \pm 0.17 \pm 0.31$
0.10-0.12	$8.50 \pm 0.15 \pm 0.16$	0.08-0.10	$8.87 \pm 0.14 \pm 0.42$
0.12-0.14	$7.38 \pm 0.14 \pm 0.31$	0.10-0.12	$5.11 \pm 0.10 \pm 0.20$
0.14-0.16	$6.27 \pm 0.12 \pm 0.33$	0.12-0.14	$3.63 \pm 0.088 \pm 0.255$
0.16-0.18	$4.52 \pm 0.10 \pm 0.13$	0.14-0.16	$2.479 \pm 0.074 \pm 0.184$
0.18-0.20	$3.267 \pm 0.084 \pm 0.149$	0.16-0.18	$1.631 \pm 0.059 \pm 0.286$
0.20-0.22	$2.429 \pm 0.072 \pm 0.202$	0.18-0.20	$1.092 \pm 0.049 \pm 0.052$
0.22-0.24	$1.748 \pm 0.060 \pm 0.149$	0.20-0.23	$0.739 \pm 0.035 \pm 0.133$
0.24-0.27	$1.277 \pm 0.042 \pm 0.090$	0.23-0.26	$0.276 \pm 0.021 \pm 0.051$
0.27-0.30	$0.811 \pm 0.033 \pm 0.061$	0.26-0.30	$0.020 \pm 0.004 \pm 0.004$
0.30-0.35	$0.262 \pm 0.013 \pm 0.047$	mean value	$0.0906 \pm 0.0003 \pm 0.0009$
0.35-0.40	$0.020 \pm 0.003 \pm 0.006$		
mean value	$0.1439 \pm 0.0004 \pm 0.0012$		

Table 5: Event shape data as for Table 4 but measured at $\sqrt{s} = 35$ GeV.

44 GeV	$1/\sigma \cdot d\sigma/dy_{23}$		35 GeV	$1/\sigma \cdot d\sigma/dy_{23}$	
0.000-0.001	15.2 ± 1.1	± 3.7	0.000-0.001	8.45 ± 0.47	± 3.23
0.001-0.002	67.4 ± 3.1	± 9.0	0.001-0.002	46.5 ± 1.4	± 3.6
0.002-0.005	86.7 ± 2.3	± 4.1	0.002-0.005	73.5 ± 1.1	± 2.7
0.005-0.010	49.4 ± 1.4	± 5.9	0.005-0.010	45.74 ± 0.67	± 2.13
0.010-0.020	16.00 ± 0.51	± 0.98	0.010-0.020	19.32 ± 0.30	± 0.66
0.020-0.030	7.26 ± 0.32	± 0.97	0.020-0.030	8.09 ± 0.19	± 0.16
0.030-0.040	4.04 ± 0.23	± 0.69	0.030-0.040	4.75 ± 0.15	± 0.30
0.040-0.050	2.35 ± 0.18	± 0.48	0.040-0.050	3.09 ± 0.12	± 0.19
0.050-0.060	1.94 ± 0.16	± 0.61	0.050-0.060	2.39 ± 0.11	± 0.14
0.060-0.080	1.302 ± 0.094	± 0.078	0.060-0.080	1.568 ± 0.060	± 0.098
0.080-0.100	0.897 ± 0.079	± 0.081	0.080-0.100	1.096 ± 0.052	± 0.109
0.100-0.130	0.601 ± 0.053	± 0.054	0.100-0.130	0.816 ± 0.038	± 0.141
0.130-0.160	0.484 ± 0.053	± 0.171	0.130-0.160	0.449 ± 0.027	± 0.048
0.160-0.200	0.276 ± 0.035	± 0.034	0.160-0.200	0.365 ± 0.023	± 0.083
0.200-0.250	0.142 ± 0.022	± 0.076	0.200-0.250	0.170 ± 0.014	± 0.039
0.250-0.400	0.024 ± 0.006	± 0.023	0.250-0.400	0.026 ± 0.004	± 0.005
mean value	0.0229 ± 0.0005 ± 0.0019		mean value	0.0266 ± 0.0003 ± 0.0015	

22 GeV	$1/\sigma \cdot d\sigma/dy_{23}$	
0.000-0.001	1.91 ± 0.87	± 2.84
0.001-0.002	18.5 ± 3.6	± 7.7
0.002-0.005	37.4 ± 3.2	± 10.7
0.005-0.010	41.4 ± 2.5	± 1.6
0.010-0.020	24.4 ± 1.4	± 3.5
0.020-0.030	11.64 ± 0.90	± 0.12
0.030-0.040	7.61 ± 0.77	± 1.57
0.040-0.050	3.76 ± 0.51	± 1.27
0.050-0.060	3.206 ± 0.490	± 0.086
0.060-0.080	2.38 ± 0.30	± 0.38
0.080-0.100	1.17 ± 0.21	± 0.81
0.100-0.130	0.85 ± 0.14	± 0.19
0.130-0.160	0.49 ± 0.11	± 0.11
0.160-0.200	0.278 ± 0.077	± 0.070
0.200-0.250	0.205 ± 0.062	± 0.066
0.250-0.400	0.022 ± 0.016	± 0.042
mean value	0.0311 ± 0.0011 ± 0.0018	

Table 6: Differential 2-jet rate D_2 at $\sqrt{s} = 44$ GeV, at 35 GeV and at 22 GeV. The values were corrected for detector and for initial state radiation effects. The first errors denote the statistical and the second the experimental systematic uncertainties.

	$1 - T$	M_H	B_T	B_W	D_2
$\alpha_s(44 \text{ GeV})$	0.1457	0.1423	0.1417	0.1278	0.1344
fit range	0.08-0.3	0.22-0.46	0.080-0.27	0.06-0.16	0.005-0.200
$\chi^2/\text{d.o.f.}$	9.4/8	31.0/5	27.1/8	48.8/4	37.8/10
Statistical error	± 0.0017	± 0.0017	± 0.0014	± 0.0016	± 0.0019
tracks only	-0.0011	-0.0012	-0.0027	-0.0004	-0.0022
clusters only	+0.0027	+0.0036	+0.0009	+0.0015	+0.0016
$\cos \theta_T$	± 0.0001	± 0.0009	± 0.0005	± 0.0008	± 0.0006
p_{miss}	± 0.0006	± 0.0008	± 0.0001	± 0.0002	± 0.0005
p_{bal}	± 0.0004	± 0.0004	± 0.0003	± 0.0004	± 0.0002
N_{ch}	+0.0002	+0.0004	+0.0003	+0.0003	+0.0006
E_{vis}	± 0.0003	± 0.0001	± 0.0003	± 0.0002	± 0.0002
fit range	± 0.0015	± 0.0032	± 0.0023	± 0.0048	± 0.0032
Experimental syst.	± 0.0032	± 0.0050	± 0.0037	± 0.0051	± 0.0040
$a - 0.225$	+0.0019	+0.0018	+0.0017	+0.0010	< 0.0001
$a + 0.225$	-0.0016	-0.0021	-0.0017	-0.0009	-0.0005
$\sigma_q - 30 \text{ MeV}$	+0.0010	+0.0001	+0.0009	+0.0007	+0.0004
$\sigma_q + 30 \text{ MeV}$	-0.0009	-0.0003	-0.0011	-0.0006	-0.0009
LUND symmetric	+0.0012	+0.0009	+0.0017	+0.0015	+0.0005
$Q_0 + 500 \text{ MeV}$	-0.0008	+0.0011	-0.0007	+0.0012	+0.0026
$Q_0 - 500 \text{ MeV}$	+0.0003	-0.0007	+0.0002	-0.0002	-0.0015
$\Lambda - 50 \text{ MeV}$	-0.0005	+0.0001	-0.0013	+0.0001	+0.0003
$\Lambda + 50 \text{ MeV}$	+0.0008	-0.0005	+0.0008	< 0.0001	-0.0011
udsc only	+0.0040	+0.0007	+0.0064	+0.0047	+0.0049
MC statistics	± 0.0011	± 0.0011	± 0.0009	± 0.0011	± 0.0012
MC modelling	+0.0050 -0.0030	+0.0033 -0.0032	+0.0072 -0.0032	+0.0054 -0.0027	+0.0067 -0.0045
$x_\mu = 0.5$	-0.0089	-0.0067	-0.0100	-0.0065	-0.0007
$x_\mu = 2.0$	+0.0115	+0.0092	+0.0125	+0.0082	+0.0045
Total error	+0.0131 -0.0101	+0.0111 -0.0091	+0.0150 -0.0112	+0.0112 -0.0088	+0.0091 -0.0063

Table 7: Values of $\alpha_s(44 \text{ GeV})$ derived using the $\mathcal{O}(\alpha_s^2)$ +NLLA QCD calculations with $x_\mu = 1$ and the $\ln(R)$ -matching scheme, fit ranges and $\chi^2/\text{d.o.f.}$ values for each of the five event shape observables. In addition, the statistical and systematic uncertainties are given. Where a signed value is quoted, this indicates the direction in which $\alpha_s(44 \text{ GeV})$ changed with respect to the standard analysis. The scale uncertainty and quark mass effects are treated as asymmetric uncertainties of α_s .

	$1 - T$	M_H	B_T	B_W	D_2
$\alpha_s(35 \text{ GeV})$	0.1510	0.1445	0.1448	0.1326	0.1448
fit range	0.08-0.3	0.22-0.46	0.080-0.27	0.06-0.16	0.020-0.200
$\chi^2/\text{d.o.f.}$	25.2/8	32.8/5	23.7/8	23.0/4	20.3/8
Statistical error	± 0.0009	± 0.0009	± 0.0007	± 0.0009	± 0.0014
tracks only	-0.0016	< 0.0001	-0.0010	-0.0006	-0.0019
clusters only	+0.0012	+0.0015	-0.0009	-0.0018	-0.0006
$\cos \theta_T$	± 0.0004	± 0.0005	± 0.0001	± 0.0002	± 0.0012
p_{miss}	± 0.0001	± 0.0001	± 0.0001	± 0.0003	± 0.0004
p_{bal}	± 0.0006	± 0.0001	± 0.0002	± 0.0006	± 0.0004
N_{ch}	+0.0006	+0.0005	+0.0005	+0.0006	+0.0005
E_{vis}	± 0.0001	± 0.0001	± 0.0001	± 0.0001	± 0.0002
fit range	± 0.0009	± 0.0017	± 0.0008	± 0.0016	± 0.0017
Experimental syst.	± 0.0021	± 0.0024	± 0.0014	± 0.0026	± 0.0030
$a - 0.225$	+0.0028	+0.0035	+0.0023	+0.0018	-0.0002
$a + 0.225$	-0.0027	-0.0033	-0.0021	-0.0020	+0.0002
$\sigma_q - 30 \text{ MeV}$	+0.0018	+0.0008	+0.0013	+0.0015	+0.0008
$\sigma_q + 30 \text{ MeV}$	-0.0015	-0.0006	-0.0012	-0.0013	-0.0004
LUND symmetric	+0.0040	+0.0034	+0.0027	+0.0029	+0.0009
$Q_0 + 500 \text{ MeV}$	-0.0006	+0.0015	-0.0014	+0.0014	+0.0024
$Q_0 - 500 \text{ MeV}$	+0.0001	-0.0006	+0.0006	-0.0008	-0.0004
$\Lambda - 50 \text{ MeV}$	-0.0008	-0.0006	-0.0021	-0.0003	+0.0009
$\Lambda + 50 \text{ MeV}$	+0.0011	+0.0007	+0.0018	+0.0003	-0.0008
udsc only	+0.0074	+0.0025	+0.0086	+0.0077	+0.0055
MC statistics	± 0.0008	± 0.0008	± 0.0007	± 0.0008	± 0.0013
MC modelling	+0.0092 -0.0054	+0.0060 -0.0055	+0.0099 -0.0048	+0.0089 -0.0045	+0.0065 -0.0034
$x_\mu = 0.5$	-0.0100	-0.0077	-0.0107	-0.0078	-0.0008
$x_\mu = 2.0$	+0.0129	+0.0103	+0.0134	+0.0097	+0.0055
Total error	+0.0160 -0.0116	+0.0122 -0.0098	+0.0167 -0.0118	+0.0134 -0.0094	+0.0091 -0.0048

Table 8: Values of $\alpha_s(35 \text{ GeV})$ derived as in Table 7 but at 35 GeV.

	D_2
$\alpha_s(22 \text{ GeV})$	0.1607
fit range	0.060-0.200
$\chi^2/\text{d.o.f.}$	1.7/4
Statistical error	± 0.0083
tracks only	+0.0023
clusters only	-0.0030
Experimental syst.	± 0.0030
$a - 0.225$	-0.0015
$a + 0.225$	+0.0010
$\sigma_q - 30 \text{ MeV}$	+0.0010
$\sigma_q + 30 \text{ MeV}$	-0.0004
LUND symmetric	+0.0034
$Q_0 + 500 \text{ MeV}$	+0.0031
$Q_0 - 500 \text{ MeV}$	+0.0001
$\Lambda - 50 \text{ MeV}$	+0.0011
$\Lambda + 50 \text{ MeV}$	-0.0009
udsc only	+0.0105
MC statistics	± 0.0025
MC modelling	+0.0116 -0.0050
$x_\mu = 0.5$	< 0.0001
$x_\mu = 2.0$	+0.0066
Total error	+0.0162 -0.0105

Table 9: Value of $\alpha_s(22 \text{ GeV})$ derived as in Table 7 but only for the differential 2-jet rate D_2 at 22 GeV.

44 GeV	$1 - T$	M_H	B_T	B_W	D_2	averaged
α_s	0.1510	0.1532	0.1681	0.1406	0.1302	0.1442
fit range	0.12-0.35	0.26-0.50	0.16-0.35	0.10-0.20	0.01-0.20	
$\chi^2/\text{d.o.f.} (x_\mu = 1)$	3.0	2.3	3.7	2.2	1.1	
x_μ fitted	0.056	0.132	0.600	0.070	0.080	
$\chi^2/\text{d.o.f.} (x_\mu \text{ free})$	2.0	2.0	3.6	2.0	1.8	
Statistical error	± 0.0028	± 0.0027	± 0.0025	± 0.0026	± 0.0021	± 0.0025
Experimental syst.	± 0.0038	± 0.0051	± 0.0036	± 0.0034	± 0.0038	± 0.0029
MC modelling	+0.0041 -0.0027	+0.0034 -0.0033	+0.0074 -0.0032	+0.0040 -0.0031	+0.0057 -0.0036	+0.0048 -0.0029
Higher orders	± 0.0241	± 0.0117	± 0.0072	± 0.0086	± 0.0036	± 0.0072
Total error	+0.0249 -0.0247	+0.0135 -0.0135	+0.0112 -0.0090	+0.0104 -0.0101	+0.0080 -0.0067	+0.0095 -0.0086

Table 10: Values of $\alpha_s(44 \text{ GeV})$ derived using the $\mathcal{O}(\alpha_s^2)$ QCD calculations with fixed $x_\mu = 1$ and x_μ fitted. The statistical and systematic uncertainties are also given.

35 GeV	$1 - T$	M_H	B_T	B_W	D_2	averaged
α_s	0.1560	0.1654	0.1699	0.1508	0.1485	0.1560
fit range	0.12-0.30	0.30-0.50	0.16-0.30	0.10-0.20	0.04-0.20	
$\chi^2/\text{d.o.f.} (x_\mu = 1)$	5.8	2.3	1.6	3.4	2.9	
x_μ fitted	0.040	0.342	0.367	0.056	0.074	
$\chi^2/\text{d.o.f.} (x_\mu \text{ free})$	2.4	2.2	0.2	1.4	3.1	
Statistical error	± 0.0015	± 0.0019	± 0.0013	± 0.0014	± 0.0020	± 0.0016
Experimental syst.	± 0.0034	± 0.0034	± 0.0025	± 0.0030	± 0.0052	± 0.0026
MC modelling	+0.0065 -0.0036	+0.0048 -0.0048	+0.0134 -0.0064	+0.0079 -0.0047	+0.0033 -0.0032	+0.0045 -0.0029
Higher orders	± 0.0279	± 0.0089	± 0.0140	± 0.0085	± 0.0068	± 0.0093
Total error	+0.0289 -0.0284	+0.0109 -0.0108	+0.0196 -0.0157	+0.0121 -0.0103	+0.0094 -0.0094	+0.0108 -0.0102

Table 11: Values of $\alpha_s(35 \text{ GeV})$ derived as in Table 10 but at 35 GeV.

(a)	$\langle 1 - T \rangle$	$\langle M_H^2/s \rangle$	$\langle B_T \rangle$	$\langle B_W \rangle$	$\langle y_{23} \rangle$	average
α_s	0.1204	0.1118	0.1158	0.1105	0.1232	0.1155
Q range [GeV]	13-172	14-172	35-161	35-161	22-161	
$\chi^2/\text{d.o.f.}$	42.6/24	10.9/14	37.4/9	21.1/9	5.0/6	
experimental	± 0.0013	± 0.0010	± 0.0018	± 0.0015	± 0.0020	± 0.0013
$x_\mu = 0.5$	-0.0050	-0.0027	-0.0039	-0.0012	-0.0043	-0.0033
$x_\mu = 2.0$	+0.0061	+0.0037	+0.0048	+0.0020	+0.0057	+0.0045
$\mu_I = 1$ GeV	+0.0023	+0.0021	+0.0056	+0.0054	—	+0.0029
$\mu_I = 3$ GeV	-0.0018	-0.0016	-0.0043	-0.0037	—	-0.0019
$a_{\mathcal{F}} \pm 50\%$	—	-0.0022 +0.0025	-0.0047 +0.0064	-0.0052 +0.0073	—	-0.0020 +0.0028
Total error	+0.0066 -0.0055	+0.0050 -0.0040	+0.0099 -0.0077	+0.0094 -0.0067	+0.0060 -0.0046	+0.0061 -0.0045

(b)	$\langle 1 - T \rangle$	$\langle M_H^2/s \rangle$	$\langle B_T \rangle$	$\langle B_W \rangle$
$\bar{\alpha}_0$	0.543	0.457	0.342	0.264
experimental	± 0.014	± 0.009	± 0.007	± 0.002
$x_\mu = 0.5$	+0.002	+0.013	+0.009	+0.030
$x_\mu = 2.0$	-0.001	-0.008	-0.006	-0.019
$a_{\mathcal{F}} \pm 50\%$	—	-0.076 +0.212	-0.036 +0.063	-0.024 +0.037
Total error	+0.015 -0.014	+0.212 -0.077	+0.064 -0.038	+0.048 -0.031

Table 12: Values of α_s (a) and $\bar{\alpha}_0$ (b) derived using the $\mathcal{O}(\alpha_s^2)$ calculations and power corrections with $\mu_I = 2$ GeV and $x_\mu = 1$. Fit ranges and $\chi^2/\text{d.o.f.}$ values for each of the five event shape observables are included. In addition, the statistical and systematic uncertainties are given. Where a signed value is quoted, this indicates the direction in which α_s and $\bar{\alpha}_0$ changed with respect to the standard analysis. The renormalisation and infrared scale uncertainties and the uncertainties due to the $a_{\mathcal{F}}$ coefficients are treated as an asymmetric uncertainty on α_s . These uncertainties are treated similarly for $\bar{\alpha}_0$ but exclude the infrared scale uncertainty.

Figures

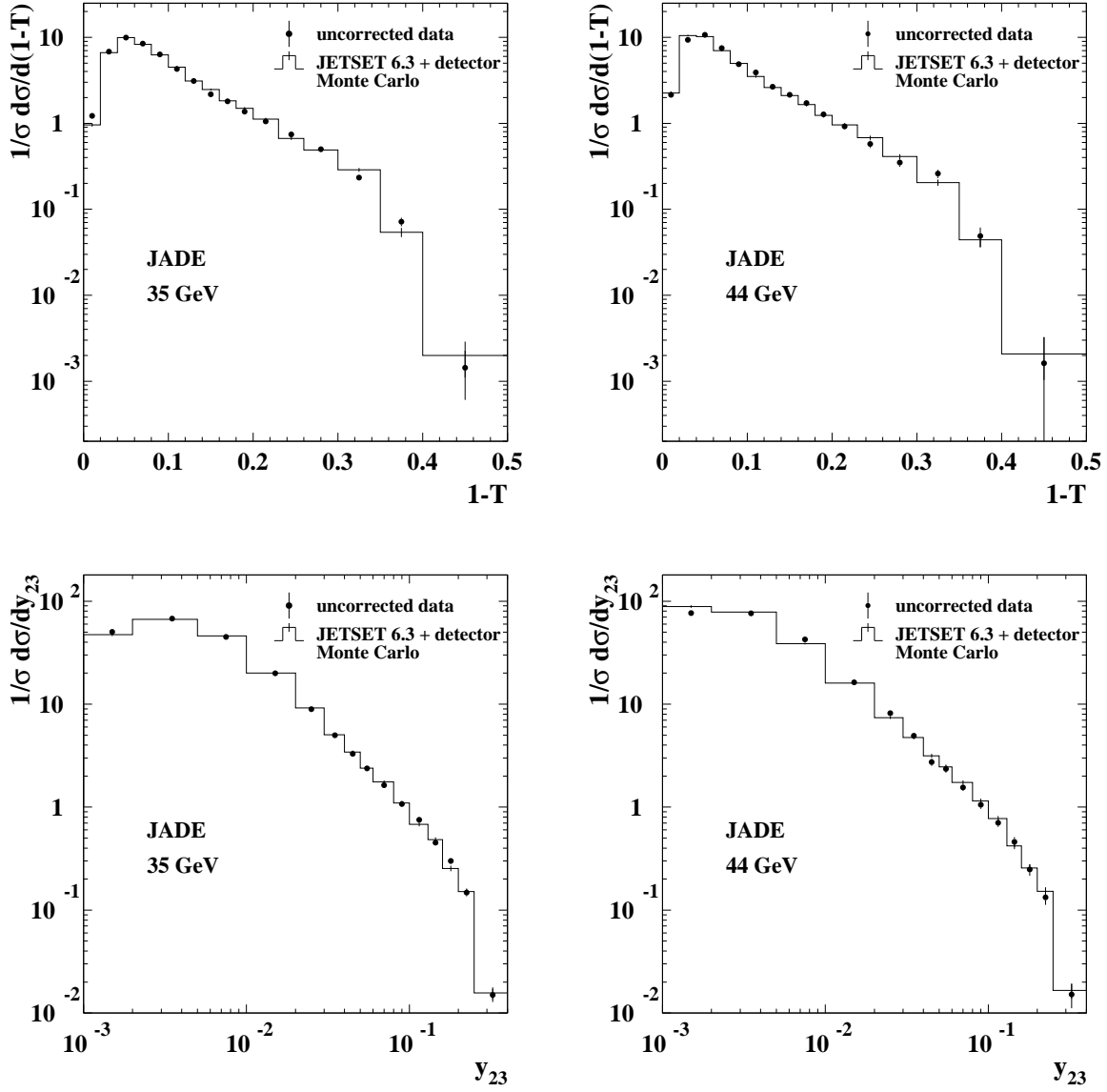


Figure 1: Measured and uncorrected distributions of the thrust observable $1-T$ (top) and of the differential 2-jet rate D_2 (bottom) at 35 (left) and 44 GeV (right). The simulated data are overlaid as a solid line histogram. Only statistical errors are shown by the error bars.

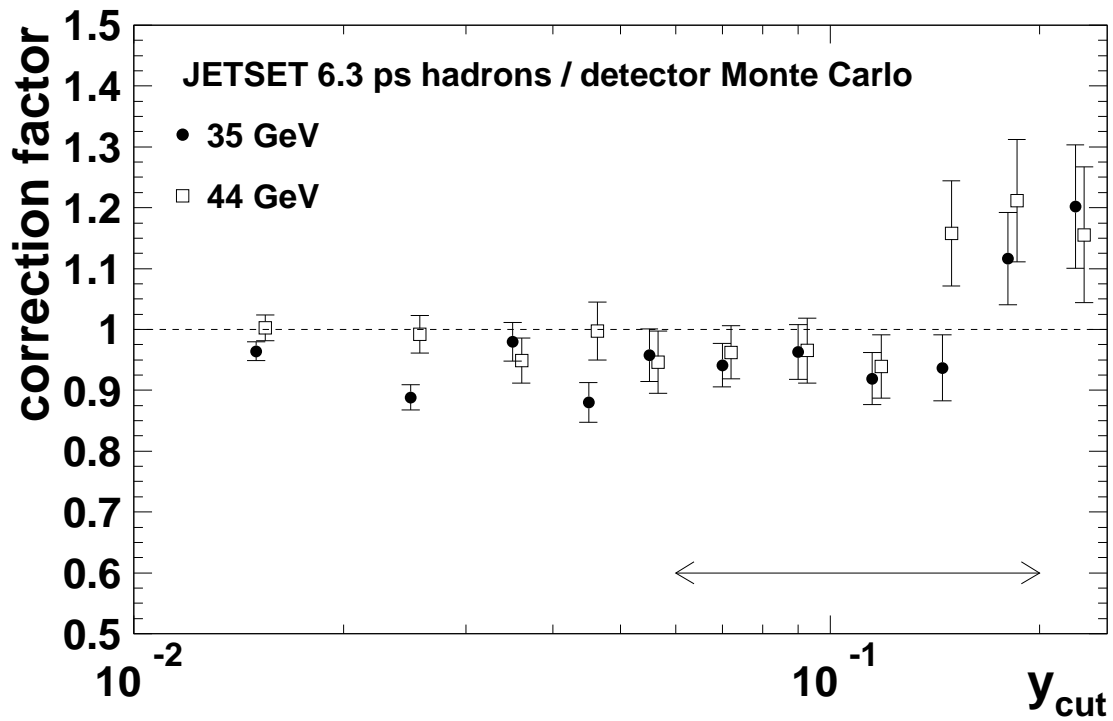


Figure 2: The detector correction factors at 35 (points) and at 44 GeV (open squares) are shown for the differential 2-jet rate, D_2 , in the Durham jet finder scheme. The error bars represent the statistical error. The arrow indicates the range of data considered to determine α_s at 22 GeV.

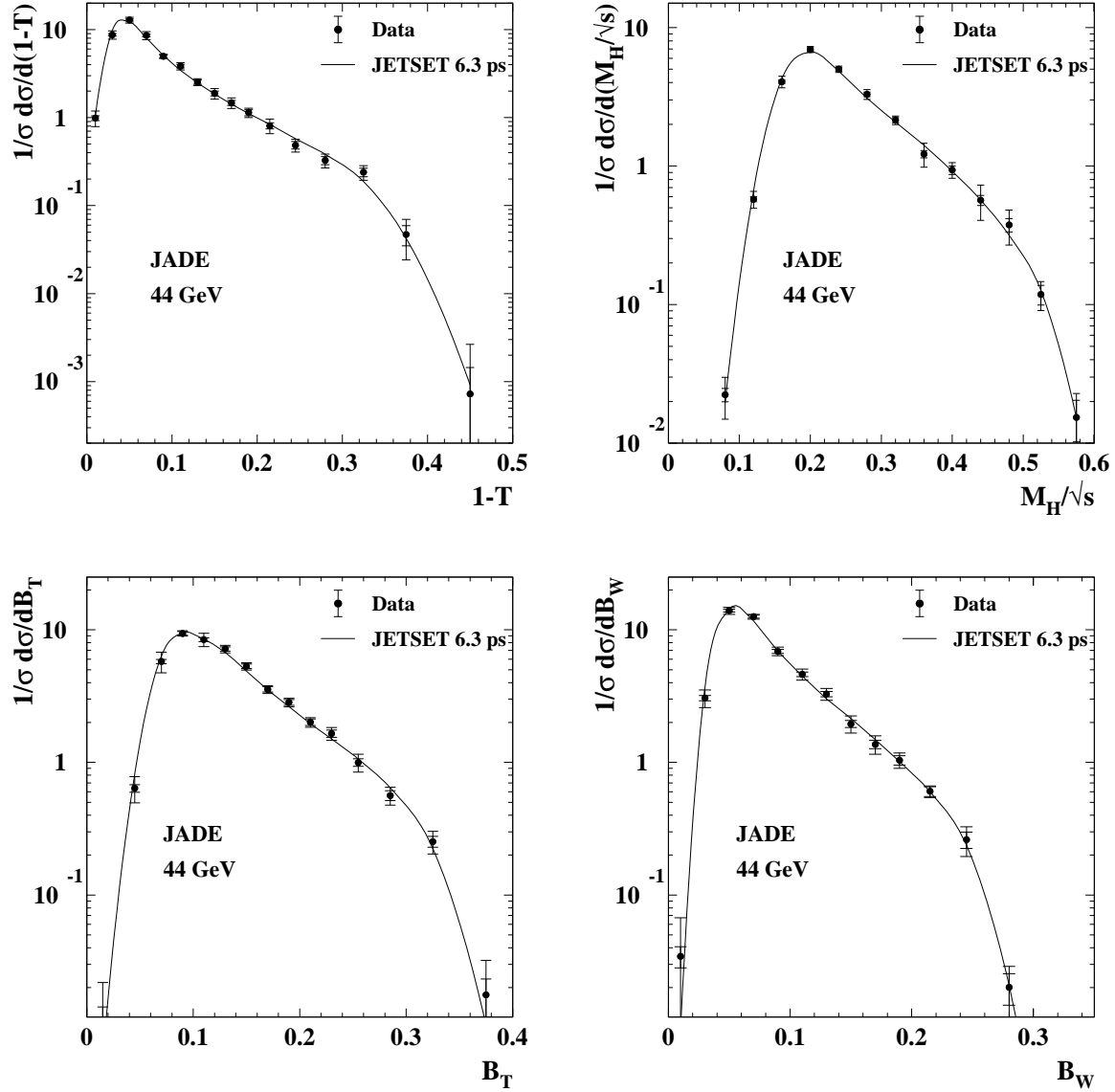


Figure 3: Event shape distributions at $\sqrt{s} = 44$ GeV corrected to the hadron level are shown for Thrust (T), heavy jet mass (M_H), total (B_T) and wide jet broadening (B_W). The error bars show the statistical error (inner tick marks) and the total error obtained by adding the statistical and experimental systematic error in quadrature. The solid line represents the JETSET 6.3 parton shower model prediction.

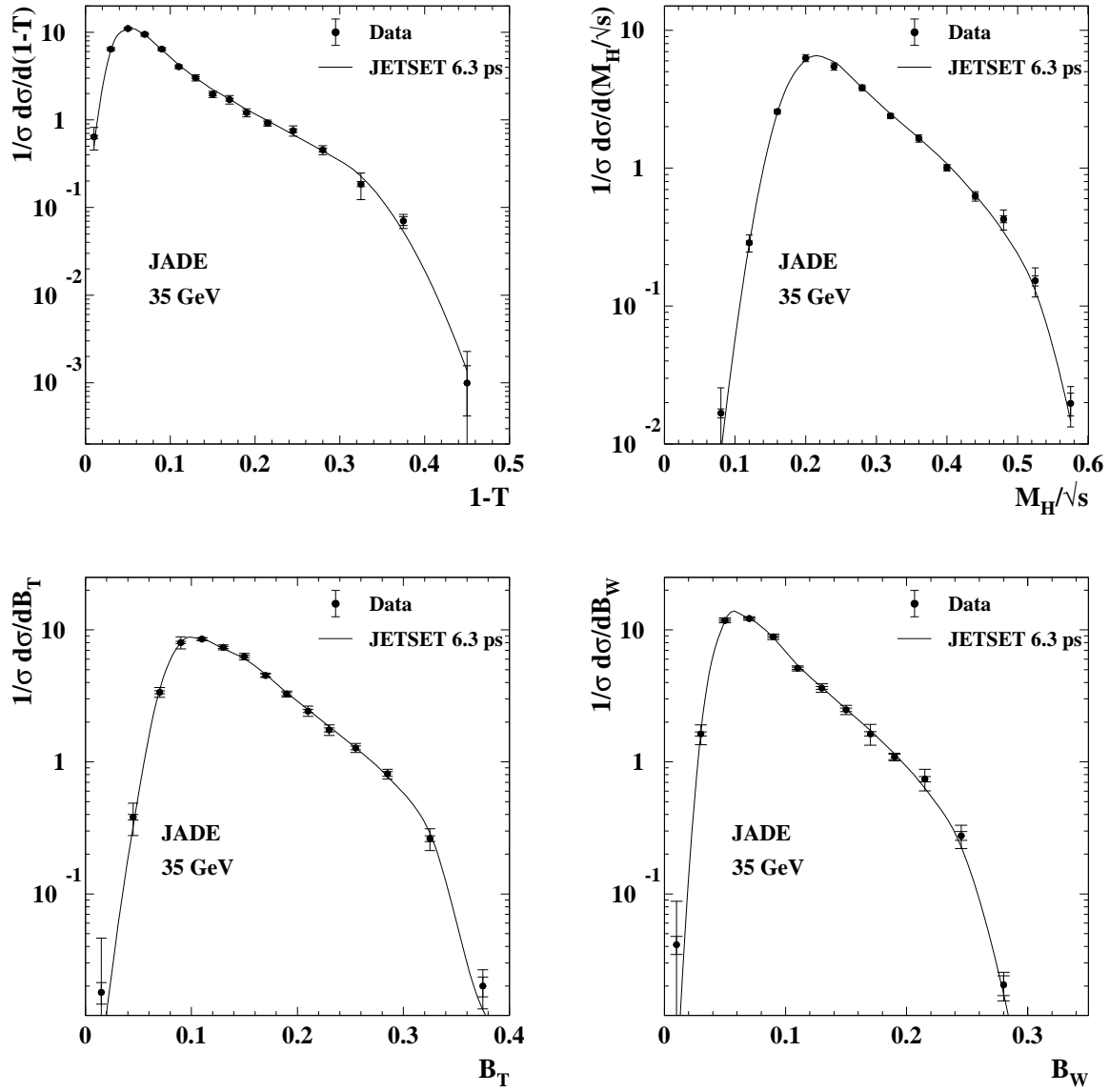


Figure 4: Event shape distributions corrected to the hadron level as for Figure 3 but at $\sqrt{s} = 35$ GeV. The solid line represents the JETSET 6.3 parton shower model prediction.

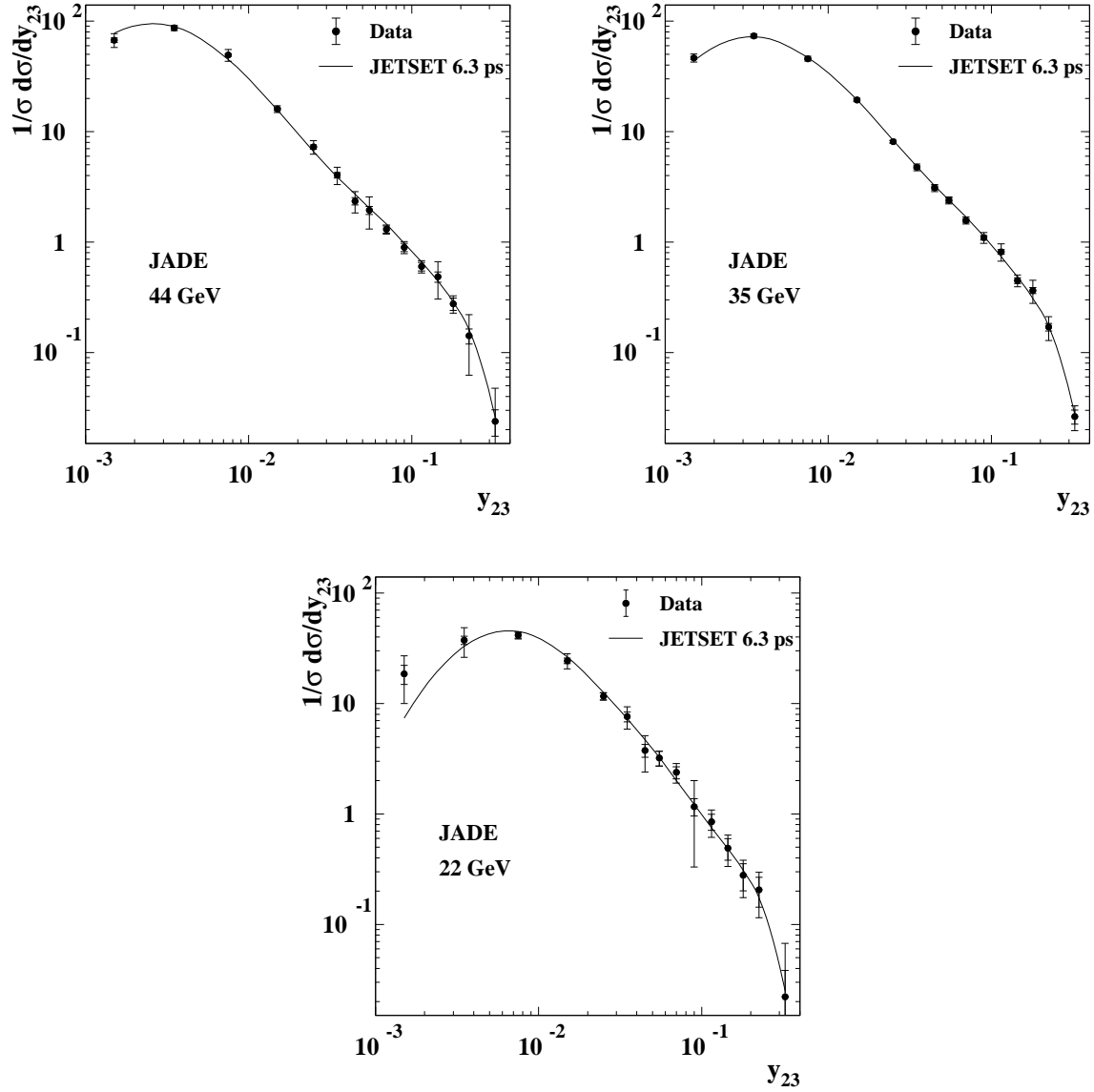


Figure 5: Event shape distributions corrected to the hadron level at $\sqrt{s} = 44, 35,$ and 22 GeV are shown for the differential 2-jet rate (D_2) in the Durham scheme. The error bars show the statistical error (inner tick marks) and the total error obtained by adding the statistical and experimental systematic error in quadrature. The solid line represents the JETSET 6.3 parton shower model prediction.

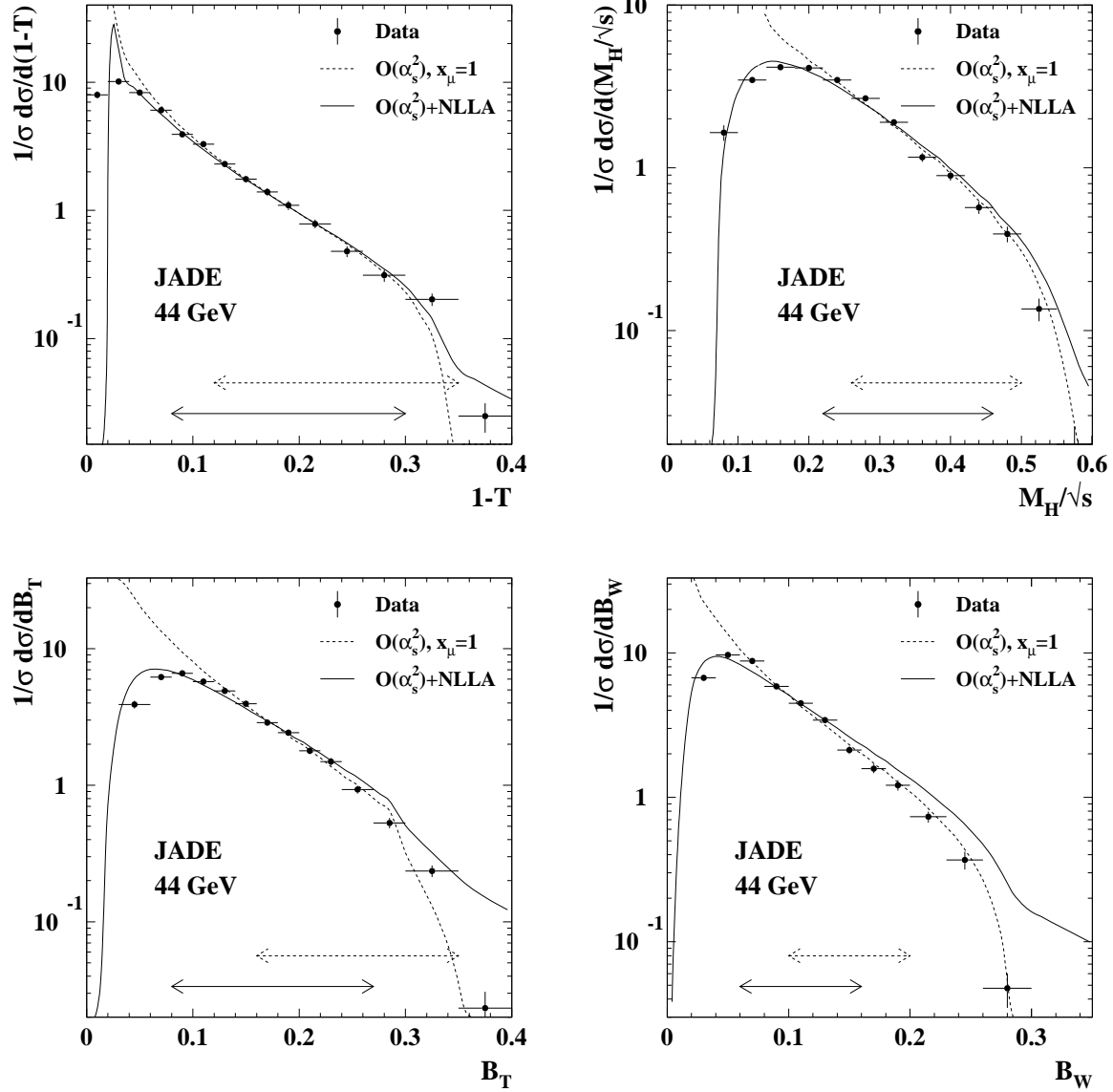


Figure 6: The distributions measured at $\sqrt{s} = 44$ GeV and corrected to parton level are shown for thrust T , heavy jet mass M_H , total and wide jet broadening B_T and B_W . The fits of the $\mathcal{O}(\alpha_s^2)+\text{NLLA}$ (solid line) and of the $\mathcal{O}(\alpha_s^2)(x_\mu = 1)$ (dashed line) QCD predictions are overlaid and the fit ranges are indicated by the solid and dashed arrows. The error bars represent statistical errors only.

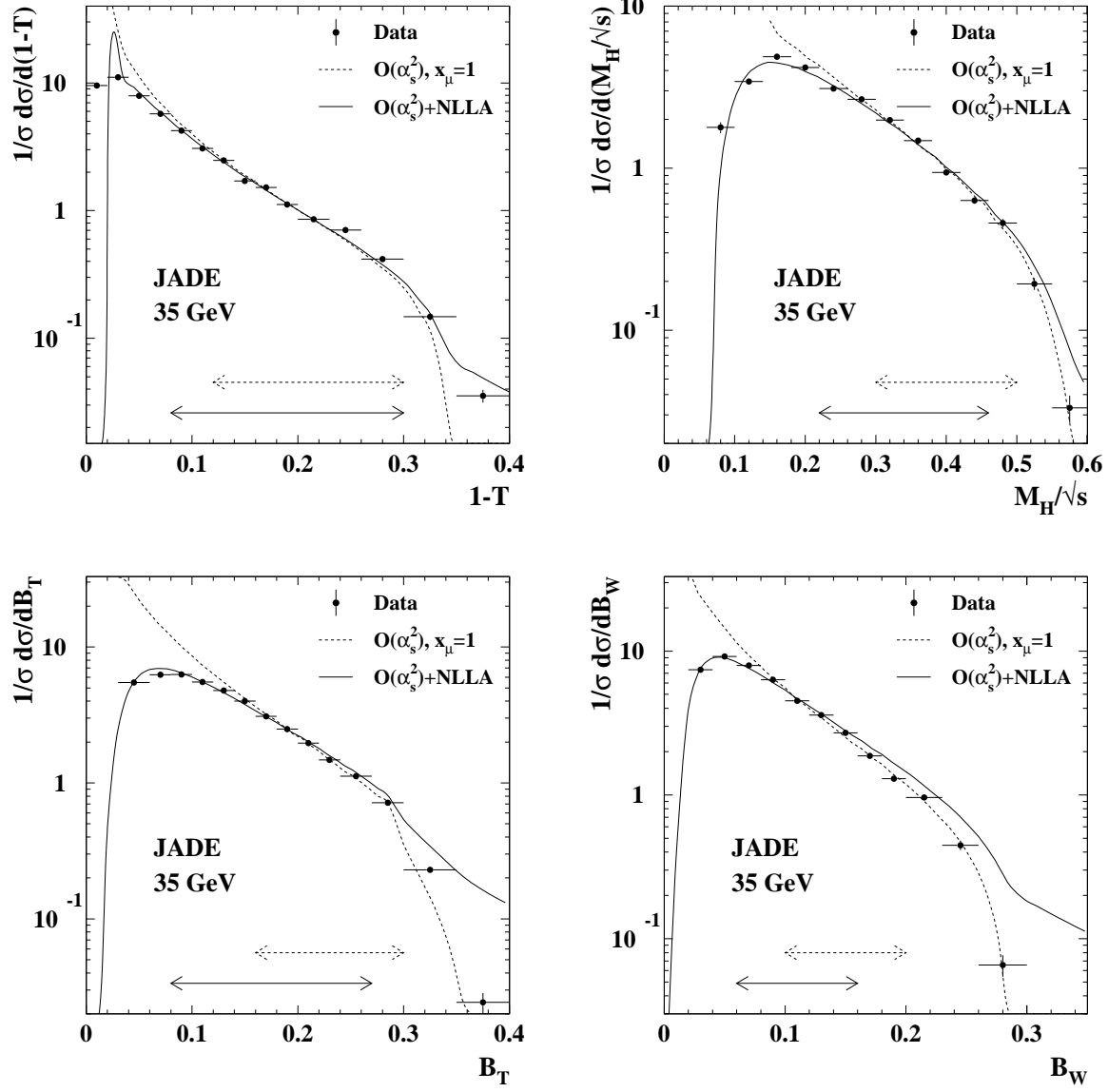


Figure 7: The same distributions as in Figure 6 but for $\sqrt{s} = 35$ GeV.

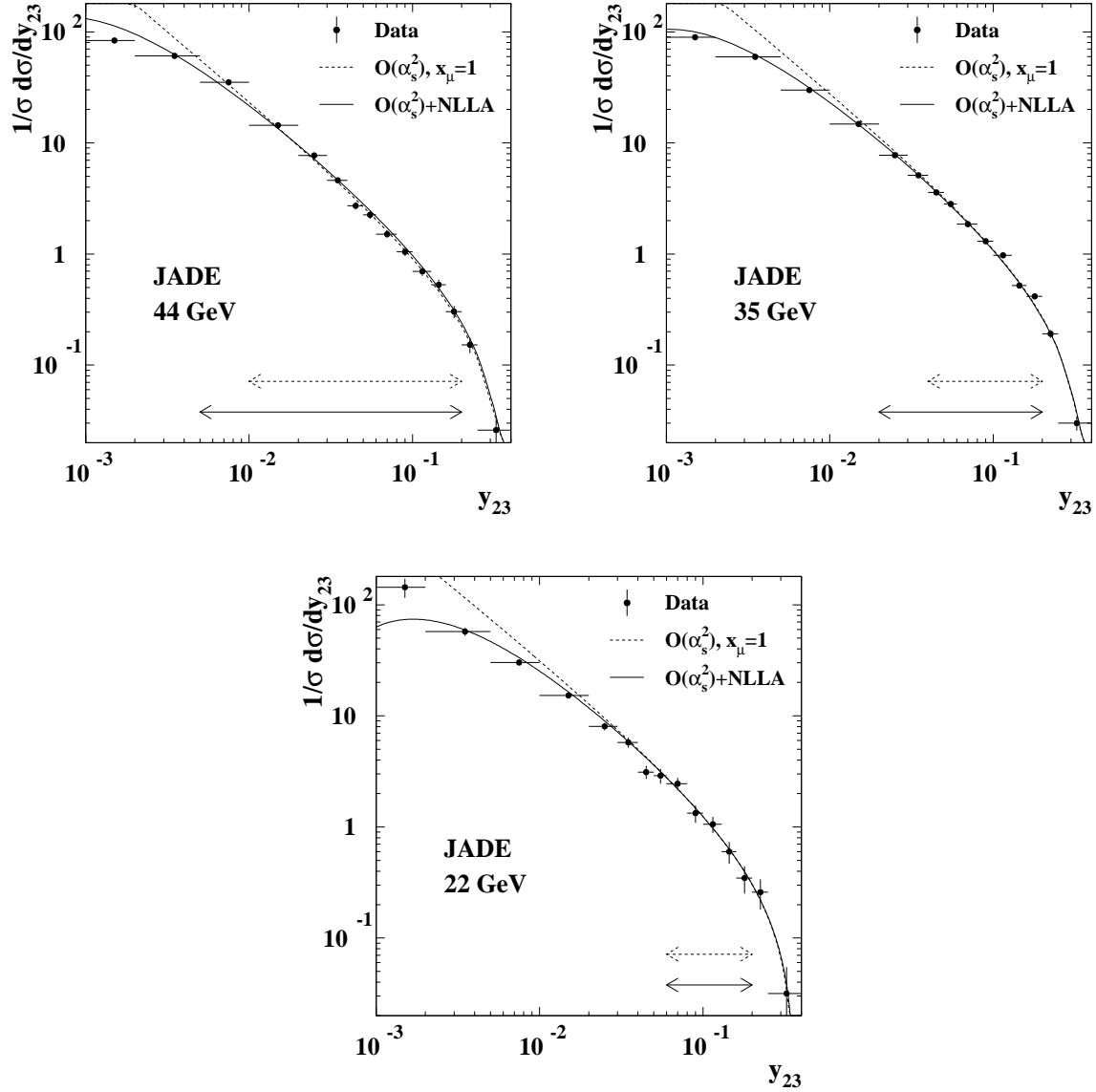


Figure 8: The distributions of the differential 2-jet rate, D_2 , measured at $\sqrt{s} = 44, 35,$ and 22 GeV using the Durham scheme are shown after correction to the parton level. The solid and dashed lines correspond to the fit results as in Figure 6.

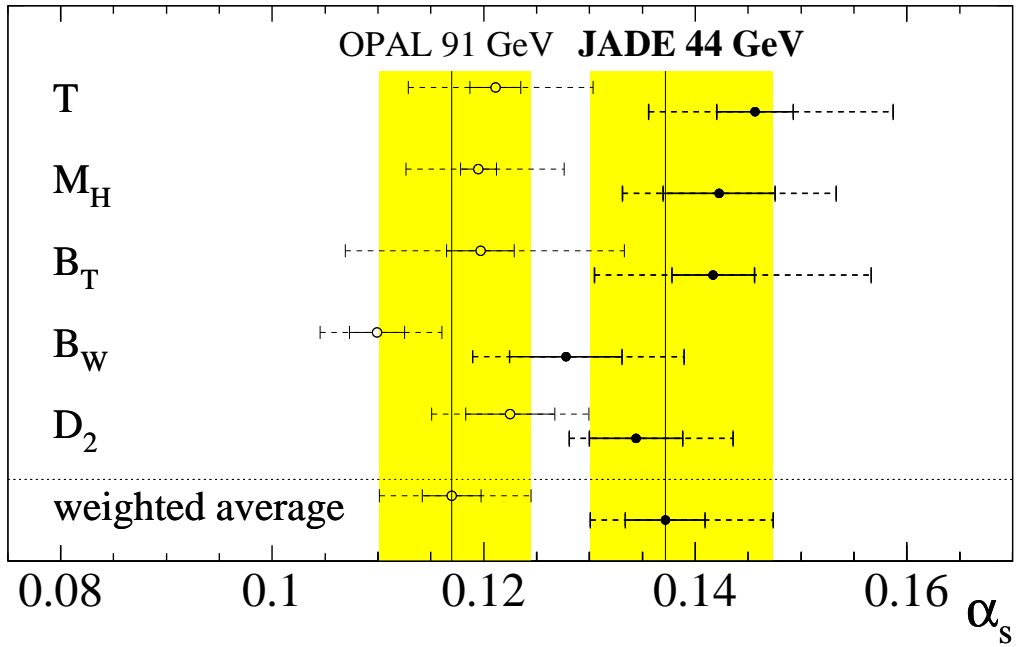
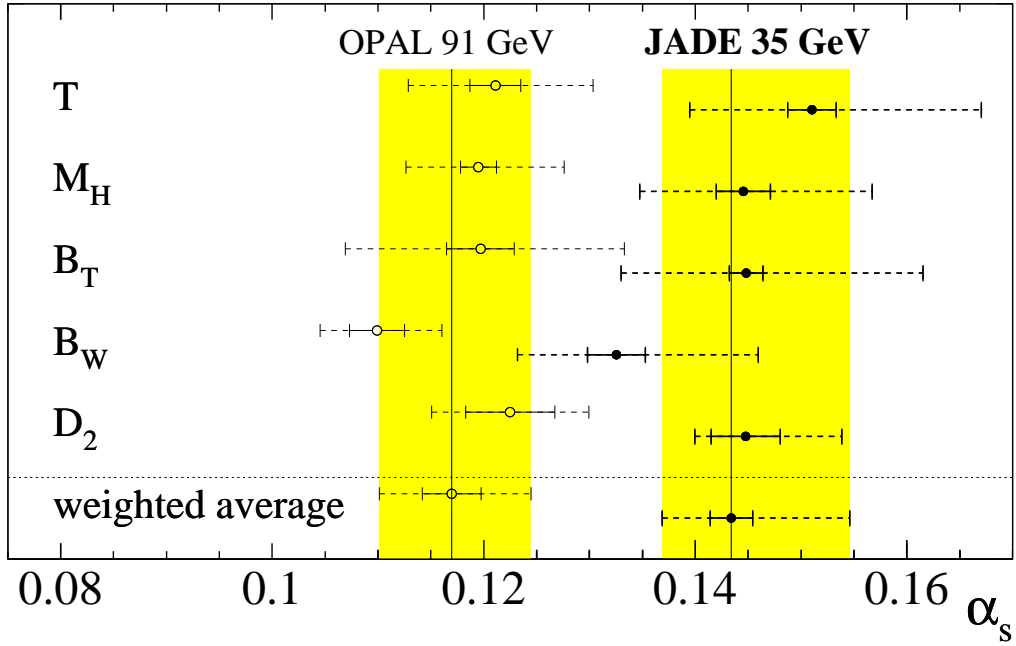


Figure 9: Values of $\alpha_s(35 \text{ GeV})$ and $\alpha_s(44 \text{ GeV})$ derived from $\mathcal{O}(\alpha_s^2)$ +NLLA fits to event shape distributions. The experimental and statistical uncertainties are represented by the solid error bars. The dashed error bars show the total error including hadronisation and higher order effects. The shaded region shows the one standard deviation region around the weighted average (see text). For comparison the α_s values and errors measured by the OPAL Collaboration [31] for the same set of observables are also shown.

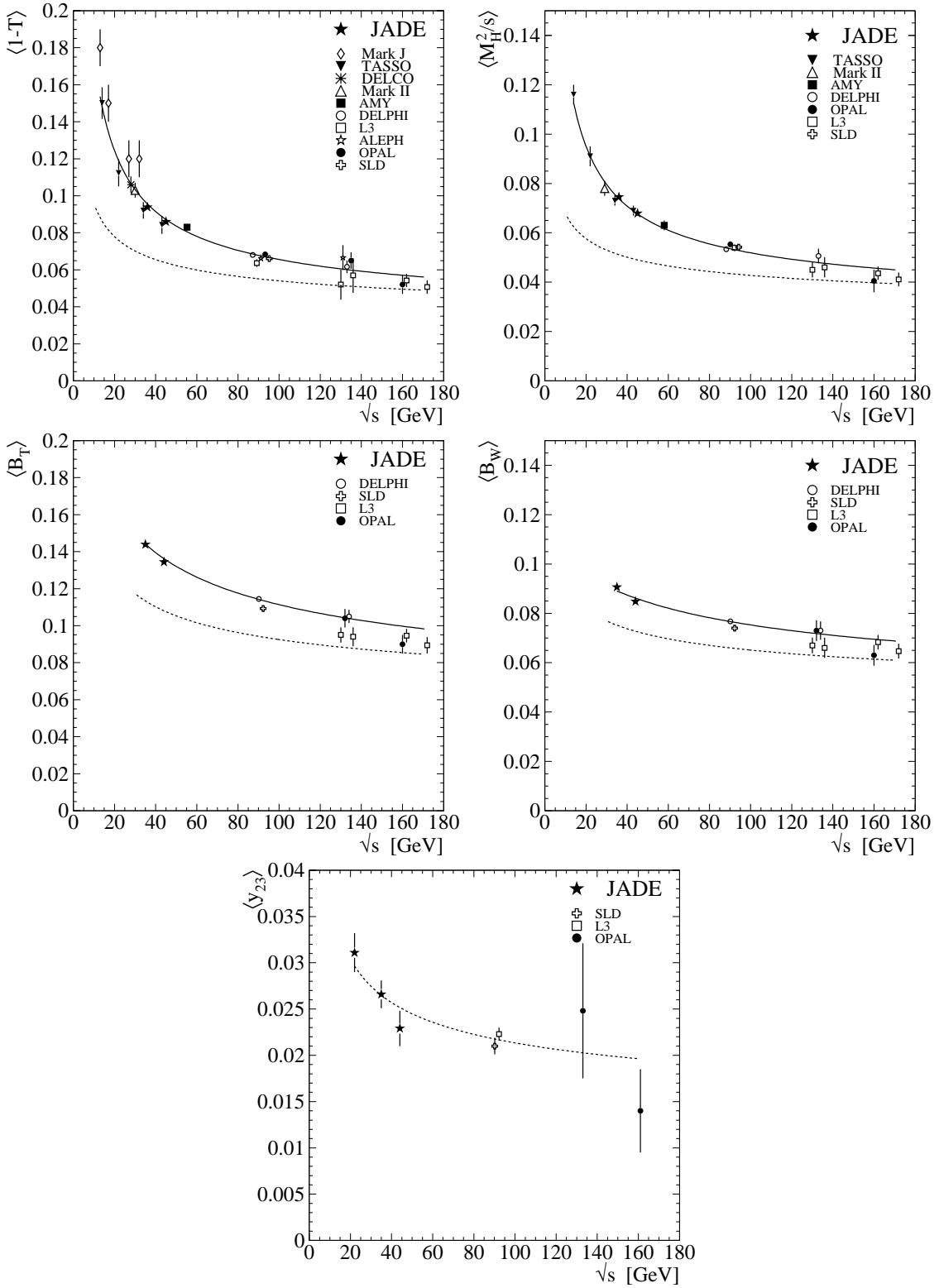


Figure 10: Energy dependence of the mean values of thrust $\langle 1 - T \rangle$, heavy jet mass $\langle M_H^2/s \rangle$, total $\langle B_T \rangle$ and wide jet broadening $\langle B_W \rangle$, and of the differential 2-jet rate $\langle y_{23} \rangle$ are shown [10,31,36,37]. The solid curve is the result of the fit using perturbative calculations plus power corrections while the dashed line is the perturbative prediction for the same value of α_s .

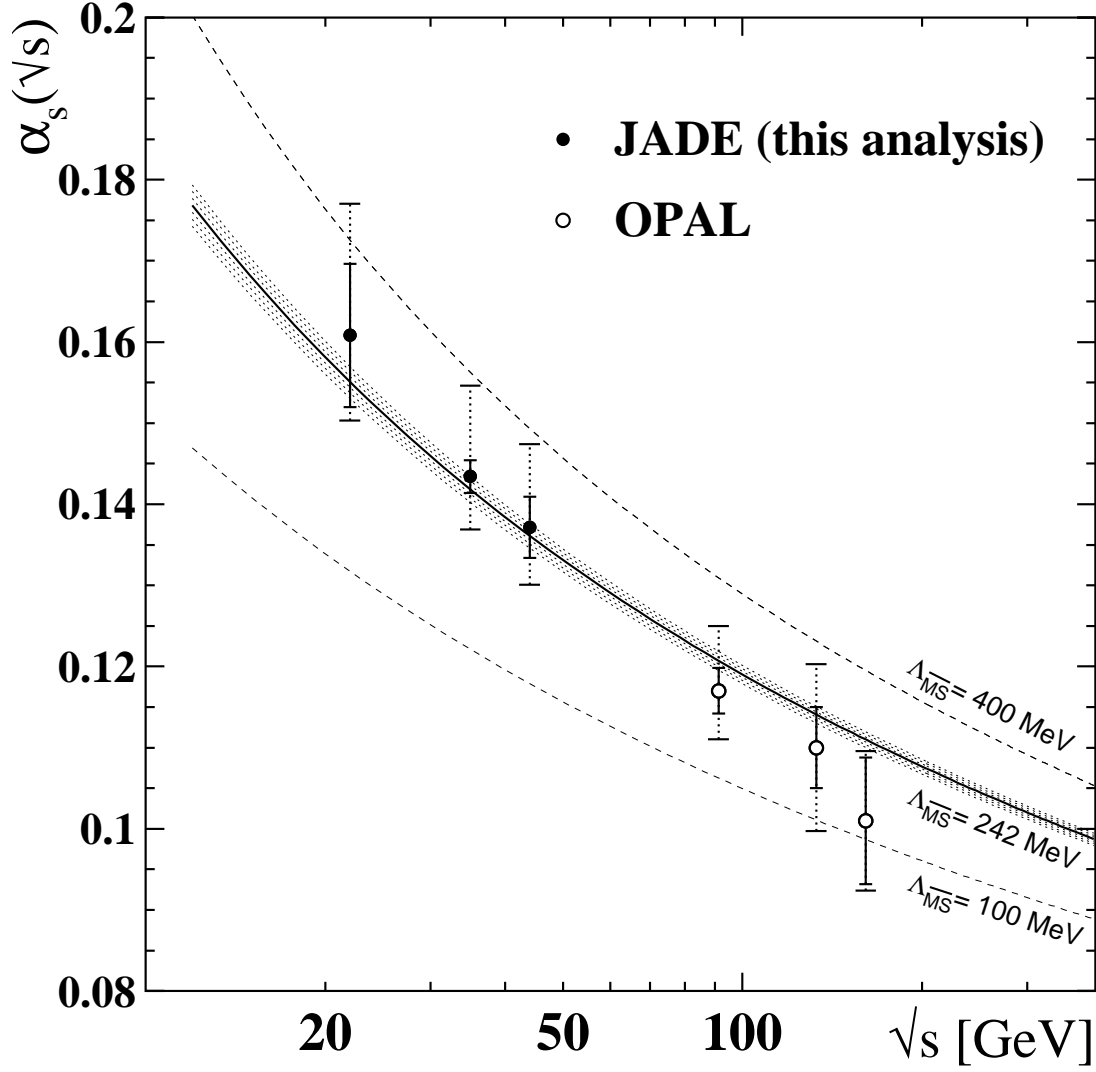


Figure 11: Values of α_s from $\mathcal{O}(\alpha_s^2)$ +NLLA fits, as a function of centre-of-mass energy. The solid error bars are the statistical and experimental uncertainties added in quadrature, the dotted error bars are the total errors. The results from OPAL [30,31] for the same set of observables are shown as representative for the LEP experiments because the relevant detector subsystems of OPAL are similar to those of JADE. The solid line and the shaded band represent the QCD prediction for $\alpha_s(M_{Z^0}) = 0.1207 \pm 0.0012$ corresponding to $\Lambda_{\overline{\text{MS}}}^{(5)} = (242 \pm 15)$ MeV which was obtained from a χ^2 fit to the data taking only experimental errors into account. For comparison the QCD predictions for $\Lambda_{\overline{\text{MS}}}^{(5)} = 100$ MeV and 400 MeV are shown by the dashed curves.